Department of Physics and Astronomy

University of Heidelberg

Diploma thesis

in Physics

submitted by

Kilian Peter Heeg

born in Ulm

2011

Models for correlated

Rydberg gases

This diploma thesis has been carried out by Kilian Peter Heeg

at the

Max Planck Institute for Nuclear Physics

under the supervision of

Herrn Priv.-Doz. Jörg Evers

Models for correlated Rydberg gases

In this thesis models for clouds of Rydberg atoms with strong interaction effects are investigated. Since the capabilities of straightforward calculations in many-body systems are limited in general, we discuss simplified models, which approximate correlations between the atoms. In addition, we present an enhanced version of the rate equation model which takes into account higher order, namely exact two-body correlations.
Different methods to improve the runtime of the models are suggested. We exploit the facts that some correlations can be neglected for large atomic seperations and that different Monte Carlo algorithms can be used to propagate into the steady state.
The models are analysed and compared from a technical and a physical point of view with the aim to decide which model is most appropriate for a given setup. We identify fundamental limitations and estimate the range of validity in the field of parameters. The models are used to calculate different observables which gives an understanding of their capabilities. In particular, we find resonance conditions in the pair correlation function and explain the super- and sub-Poissonian characters of excitation counts.

Modelle für korrelierte Rydberggase

In dieser Arbeit werden Modelle für stark wechselwirkende Rydberggase untersucht. Da im Allgemeinen die Möglichkeiten einer direkten Simulation in Vielteilchensystemen limitiert sind, betrachten wir vereinfachte Modelle, welche die Korrelationen zwischen Atomen annähern. Außerdem stellen wir eine erweiterte Version des Ratengleichungsmodels vor, die auch Korrelationen höherer Ordnung, nämlich exakte Zweiteilcheneffekte miteinbezieht.
Es werden verschiedene Methoden vorgestellt, die die Laufzeit der Modelle verbessern. Dazu nutzen wir aus, dass Korrelationen für große Atomabstände vernachlässigt oder andere Monte-Carlo-Methoden für die Propagation in den Endzustand verwendet werden können.
Die verschiedenen Modelle werden sowohl von einem technischen als auch physikalischen Blickpunkt aus analysiert und verglichen, um entscheiden zu können, welches Modell für welche Situation am besten geeignet ist. Wir ermitteln die fundamentalen Limitierungen und schätzen den Gültigkeitsbereich bezüglich der Parameterwahl ein. Die Modelle werden verwendet, um mehrere Observablen zu berechnen. Insbesondere finden wir Resonanzen in der Paarkorrelationsfunktion sowie sub- und superpoissonischen Eigenschaften in der Verteilung der Anregungszahlen.

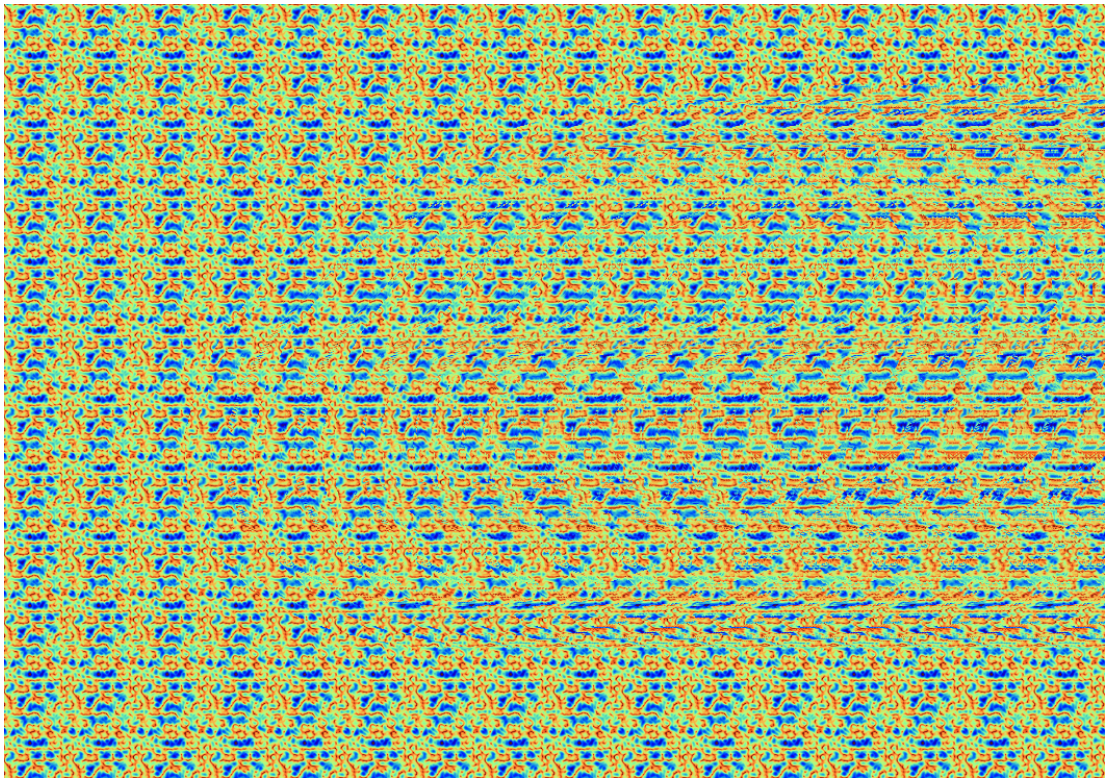

Contents

1 Introduction

1.1 Overview

Rydberg atoms and their properties have been studied for several decades [Gal94]. They are of particular interest because of some distinctive characteristics: their large size, long lifetime and probably most important, huge dipole moments. These dipole moments lead to strong interaction effects between the atoms. Due to a large polarizability the shape and strength of interactions is tunable with external electric fields [Vog06a]. In the last years the rapid development of advanced trapping and cooling mechanisms gave rise to intense studies of clouds of ultracold Rydberg atoms. At low temperatures the movement of the atoms during a typical experimental timescale can be safely neglected, which is called the frozen Rydberg gas approximation [AVG98]. This makes it possible to study the long range interactions in such a cloud without the problems of disturbance and noise by too many atomic collisions. At moderate densities in the experiments of $n_{3\mathrm{D}} = 10^9 - 10^{10}/\mathrm{cm}^3$, the interaction between atoms in their ground state can be neglected, while the strong effects in the Rydberg states result in interesting many-body effects. Newer experiments can produce Rydberg excitations in Bose-Einstein condensates [Hei08]. For example, the Heidelberg experiment reaches densities of about $10^{14}/\mathrm{cm}^3$ with Rubidium atoms at a temperature of 260 nK [Whi11].

Strong interactions between a small number of atoms as well as collective many-body effects led to a vast range of ideas and applications in different fields of physics in the last years. Especially the effect of the dipole blockade, the suppression of multiple Rydberg excitations, was utilized to suggest an implementation for quantum logic gates [Jak00; Luk01]. The few particle behaviour of a Rydberg system could be observed in [Gaë09; Urb09] and a CNOT gate could be realized in [Ise10]. Closely related are the ideas of a quantum simulator with Rydberg atoms [Wei10] as well as long distance quantum communication [PM09]. Moreover, the formation of a crystalline structure was discussed [PDL10]. In the field of quantum optics generation of non-classical light states like single photon sources or correlated photon emission [SW02; PAM11] have been proposed. Ultimately, the cooperative non-linear effects in Rydberg EIT systems attracted a lot of attention [Pri10; Sev11a; Sev11b; POF11].

Next to the experimental challenge it is also very important to describe the phenomena with accurate models. For this, several different approaches have been suggested. A straightforward many-body simulation collapses due to the exponential scaling laws in runtime and memory requirements with respect to the atom number. To overcome this, one can use symmetries or neglect certain states in the Hilbert space and then calculate the exact Hamiltonian dynamics. These models work very well in the high density regime, that means if the interaction between many atoms is very strong [RH05; You09]. However, for moderate or low densities these techniques are not suited due to their rapidly increasing runtime. For such experimental settings other models have to be used. Starting from a few atom description one can use different simplifications and assumptions and then expand the model to higher atom numbers. For example, all

correlations between atoms are neglected in mean-field models. Such techniques could describe a lot of earlier experiments [Ton04; Wei08; Cho08], but more complicated observables required the development of more sophisticated models: The cluster expansion model from [Sch10] includes, in contrast to the mean-field models, exact two-body correlations, but uses simplified expressions for higher orders. A completely different method was introduced in [Ate07b]. Here the basic equations are transformed such that the system can be solved with Monte Carlo techniques. However, the interaction effects between atoms are included in an approximate way. This prevents the model from computing exact two-body correlations.

The aim of this work is to analyse these simplified models. Given an experimental setup, it is not always clear which model should be used to describe the physics best. Thus, it is important to obtain a better understanding of their ranges of validity in terms of both a technical and a physical point of view. To this end we implement these existing models on our own. Moreover, this allows to compare different aspects and properties of the models, such as their runtime.

In addition, we develop an enhanced model which is based on the rate equation. While the rate equation does not include exact two-body correlations, it is an obvious step to take these effects into account. In this sense our improved model, the Hybrid model, can be seen as a similar improvement to the rate equation as the cluster expansion to the mean-field models.

This thesis is structured as follows: We begin to introduce the most important properties of Rydberg atoms for our case in the next sections 1.2.1 and 1.2.2. Then we give an overview on existing models and their derivation (chap. 2). In chapter 3 we take a closer look on the interaction between Rydberg atoms and analyse which effects are of importance for our purposes. Several runtime improvements for the models are presented in chapter 4, whereas we develop a new model in chapter 5. The models' capabilities are then discussed from a technical (chap. 6) as well as from a physical point of view (chap. 7). In the latter we also focus on interesting observables and give some new results. We conclude with a summary and an outlook in chapters 8 and 9.

1.2 Rydberg Atoms

1.2.1 Properties

Rydberg atoms, named after Johannes Rydberg (1854-1919), are atoms where (at least) one electron is excited to a high principal quantum number n. Since many characteristics in atomic physics scale with n, Rydberg atoms have "exaggerated properties" [Gal94] which can be found in [Gal94; CP10; SWM10], for example. The first one to mention is their giant size: The radius scales like $a_0 n^2$. Because of this size, semi-classical theories such, as the Bohr model, can be applied to a good degree. For high angular quantum numbers l the electronic shell structure is far from the core and the properties are very close to the Bohr model's predictions. For instance, the binding energy scales with $1/n^2$ and the energetic separation with $1/n^3$. For a lower angular quantum number l the electron can penetrate the inner shells of the atom and the binding energy becomes larger. The binding energy can then be described with an effective quantum number $n_{\text{eff}} = n - \delta_{n,l}$ [Dem05]. As reported in [Ste07] radio recombination lines in carbon with principal quantum numbers of $n \sim 1009$ have been observed in stellar objects, which corresponds to an atomic size of 0.1 mm.

In addition to their size, Rydberg atoms have huge dipole moments. Their values can be estimated to $\sim n^2 \cdot ea_0$, originated from the Hydrogen atom theory. The large dipole moments are the key for strong couplings of Rydberg states and interatomic interactions. Moreover, Rydberg states are very sensitive to external electric fields: Their polarizability scales like n^7, which makes the energy of the Stark-shifted states easily tunable. Hence, so called Förster-resonances can be adjusted, which makes it possible to change the interaction between the atoms in their absolute value as well as in their radial and angular dependence [Car04; Vog06a].

The usual lifetime of low n states is of the order of a few nanoseconds. In contrast, Rydberg states decay much slower. The scaling with the principal quantum number is approximately $\tau \sim n^3$. This makes Rydberg states accessible to experiments very well: The states can be probed by a laser for a rather long time and have, in addition, a small linewidth.

All these properties are also listed in the following table:

property	**n dependence**
radius	n^2
binding energy	n^{-2}
energy between adjacent states	n^{-3}
dipole moment	n^2
polarizability	n^7
lifetime	n^3

1.2.2 Rydberg Blockade

One of the most fascinating effects of Rydberg atoms is the Rydberg or dipole blockade [Luk01], which leads to many interesting applications in quantum information theory and quantum optics. It arises from dipole couplings between different Rydberg levels and eventually leads to energy shifts of multiply excited states. An example for two atoms can be seen in figure 1.1. A laser couples to these atoms and can excite them into Rydberg states. If the two atoms are far apart from each other, the dipole-dipole

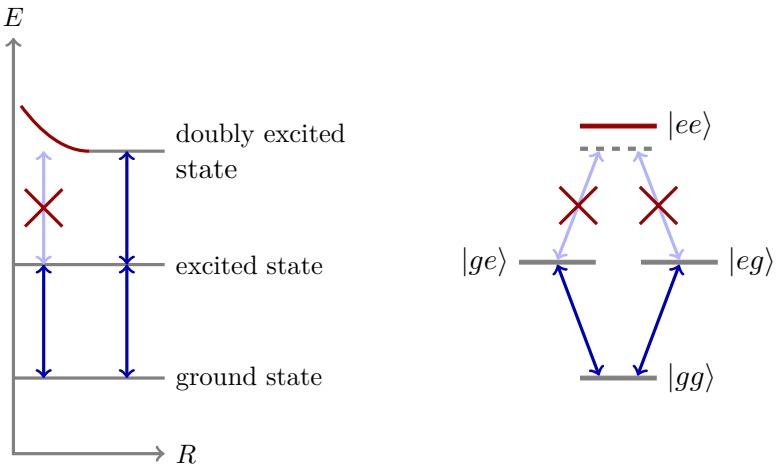

Figure 1.1: Rydberg blockade with two atoms: The double excitation is prohibited at small separations.

interaction is negligible and the doubly excited state can be populated. However, for small distances an interaction induced energy shift appears due to the dipole-dipole potential. Usually, this is a van-der-Waals potential, scales with n^{11} and is therefore very pronounced for Rydberg atoms (a more detailed discussion of the interaction is given in chap. 3). The doubly excited state is then shifted out of resonance with respect to the laser frequency. This allows only one excitation to be in the system, multiple excitations are blockaded. This could be observed in [Gaë09; Urb09] for the case of two atoms.

A direct consequence of this blockade can be seen in the excitation dynamics. A single atom driven by a resonant laser performs Rabi oscillations with a laser and atom dependent frequency Ω [SZ97]. If the ground state $|g\rangle$ and the excited state $|e\rangle$ are coupled by this coefficient, one observes the population inversion:

$$W_1(t) = P_{|e\rangle} - P_{|g\rangle} = -\cos(\Omega \cdot t) \tag{1.1}$$

Two independent atoms, in our case atoms with a large separation, perform this oscillation in the same time, which results in:

$$W_{2,\text{ind.}}(t) = 2 \cdot W_1(t) = -2 \cdot \cos(\Omega \cdot t) \tag{1.2}$$

Now we consider the case where the doubly excited state is shifted out of resonance due to the Rydberg blockade. Then we can neglect it and only use the states $|gg\rangle$, $|eg\rangle$ and $|ge\rangle$ in the calculation. After a basis transformation one finds that the symmetric state $|+\rangle = \frac{1}{\sqrt{2}}(|eg\rangle + |ge\rangle)$ is coupled to the ground state $|gg\rangle$ not by the factor Ω, but by $\sqrt{2} \cdot \Omega$, while the antisymmetric state $|-\rangle = \frac{1}{\sqrt{2}}(|eg\rangle - |ge\rangle)$ is not coupled to any other state at all. Consequently, we see a Rabi oscillation with

$$W_{2,\text{coll.}}(t) = P_{|+\rangle} - P_{|gg\rangle} = -\cos(\sqrt{2} \cdot \Omega \cdot t) \tag{1.3}$$

which has a different period than in the independent case. In fact, this effect could nicely be seen in [Gaë09]. The faster oscillation is a sign of collective behaviour. In this case one can only think in terms of entangled atoms and collective states $|+\rangle$ and $|-\rangle$. Note that for small times the total probability to find an atom in an excited state is the same for the independent and the collective case, because the Rydberg states are hardly populated and the interaction effects do not appear yet:

$$P_{\text{ind.}} = 2 \cdot P_{|e\rangle} = 2 \cdot \sin(\Omega t)^2 \approx 2(\Omega t)^2 \tag{1.4}$$

$$P_{\text{coll.}} = P_{|+\rangle} = \sin(\sqrt{2}\Omega t)^2 \approx 2(\Omega t)^2 \tag{1.5}$$

The discussed effects do not only occur for two, but also for N atoms. If all atoms are very close, all multiply excited states are shifted out of resonance such that only one excitation is present in the system. In this limit one can perform simple calculations with the ground state $|g_1 g_2 \dots g_N\rangle$ and the Dicke state $\frac{1}{\sqrt{N}} \sum_i |g_1 \dots e_i \dots g_N\rangle$. Since all atoms can be reduced to this single two-level system the term “superatom” is used [SC09].

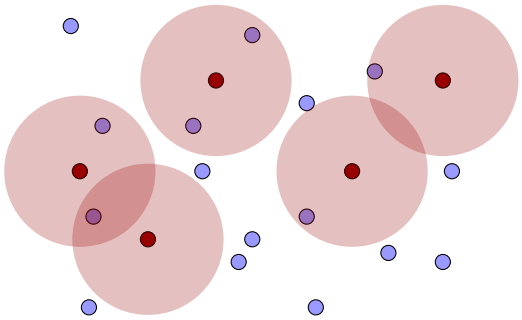

Figure 1.2: Rydberg blockade radius: Further excitations in the vicinity of Rydberg excitations are blockaded.

In general the blockade effect does not cover the whole atomic cloud and the system can contain several excitations. However, in a certain distance around these Rydberg atoms no further atoms can be excited as it is shown in figure 1.2. Depending on the interaction strength a blockade radius or a blockade volume in which only one excitation is possible, can be defined (sec. 7.3). As the density of the atom cloud increases, the number of Rydberg excitations should therefore saturate at some point. This could be observed in many experiments, such as [Sin04; Ton04].

2 Theoretical Background

In the last few years several models have been developed to describe a cloud of Rydberg atoms. In this chapter we want to introduce the concepts behind those models. We start with some definitions and derive a master equation which includes all relevant processes. After this we explain why it cannot be used in general and how the simplified models emerge from the master equation.

2.1 Notation, Units & Setting

In most of the experiments a two step excitation scheme is used to excite atoms to Rydberg states. This means, starting from a ground state $|g\rangle$ ($5s$ in case of Rb), the atom can be excited to an intermediate state $|m\rangle$ (typically $5p$ for Rb), which is then coupled to a Rydberg state $|r\rangle$. We use this notation whenever it is possible. Otherwise we use numbers to denote the states (see fig. 2.1). Sometimes the intermediate state is far detuned, then the state can be adiabatically eliminated and the system reduces to a two-level system.

For an accurate description all three states have to be considered in general.

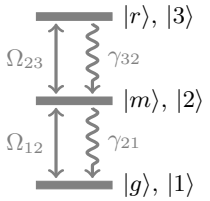

Figure 2.1: A three level system is the usual level scheme.

The coupling between the atomic states is realized with laser fields. Their most important parameter is the Rabi frequency:

$$\Omega_{ij} = \frac{|\vec{d}_{ij}|\mathcal{E}}{\hbar} \tag{2.1}$$

Here $\mathcal{E}$ is the laser amplitude and $\vec{d}_{ij}$ is the transition dipole moment. In essence these frequencies describe the strength of the laser coupling. Note that these laser fields are treated classically.

In general the laser frequency ω_{ij} does not match the transition frequency of the states $|i\rangle$ and $|j\rangle$, so we introduce the laser detuning Δ_{ij}:

$$\Delta_{ij} = \omega_{ij} - |E_i - E_j| \tag{2.2}$$

Most of the time we are only interested in Δ_{23} which we will abbreviate with Δ. Unless otherwise stated, the detunings are always zero.

Moreover, we have to include the spontaneous emission: The parameters γ_{32} and γ_{21} are the decay rates of the corresponding transitions. Note that γ_{32} is very small compared to all other parameters (see sec. 1.2.1).

Finally, we take into account dephasing between states $|i\rangle$ and $|j\rangle$, which might occur due to instabilities in the experiment, the finite laser line width or Doppler effects. We abbreviate these dephasing rates with Γ_{ij}.

In some parts of this work we also consider a two level scheme: a ground state $|g\rangle$ is directly coupled to a Rydberg state $|r\rangle$. In this case the notation is straightforward: the indices of Ω, Δ, γ and Γ can be dropped since only one transition is present in the system.

Typical values for the parameters Ω, Δ, γ and Γ are in the range of MHz. Thus, we use 1 MHz as our basic unit for frequencies. In addition we give the interaction energy in terms of MHz. In the same time our basic time unit becomes $1\,\mu$s. As the basic length unit we use $1\,\mu$m, because this is about the order of magnitude for typical particle distances. All parameters in this work are given as multiples of these basic units.

In general we are interested in modelling a large cloud of atoms. The number of interacting atoms in experiments is usually quite large: several 10^3 [Pri10], 10^4 [You09] or even higher. For an accurate description the models should ideally be able to cover the same amount of atoms. This is not always possible, such that we have to average over the outcome of different spatial realizations. By this we can obtain quite precise results in our simulations. We do not restrict the geometry here since we are interested in random samples in different trap dimensions as well as in atoms in lattice structures.

2.2 The Master Equation

The time evolution of a quantum mechanical system is given by the Schrödinger equation [Sch04]. However, a plain Schrödinger equation does not include spontaneous emission or other dephasing effects between the atomic states. To include these processes we have to use a density matrix based approach.

The fundamental equations for the later discussion are obtained from a master equation which describes the time evolution of the density matrix of our system. The time evolution consists of coherent and incoherent parts. The coherent part contains the Hamilton operator of the system. For a three-level system with ground state $|g\rangle$, intermediate state $|m\rangle$ and Rydberg state $|r\rangle$ the Hamiltonian for atom i can be written as:

$$\begin{aligned} H^{(i)} &= H_0^{(i)} + H_{\text{Laser}}^{(i)} \\ &= \hbar\Delta_{12}^{(i)} |g\rangle^{(i)(i)}\langle g| - \hbar\Delta_{23}^{(i)} |r\rangle^{(i)(i)}\langle r| \\ &\quad + \hbar\frac{\Omega_{12}^{(i)}}{2}\left(|g\rangle^{(i)(i)}\langle m| + h.c.\right) + \hbar\frac{\Omega_{23}^{(i)}}{2}\left(|m\rangle^{(i)(i)}\langle r| + h.c.\right) \end{aligned} \tag{2.3}$$

The Δ in the first line denotes the laser detuning between the states $|g\rangle$ and $|m\rangle$, and $|m\rangle$ and $|r\rangle$, respectively. The Rabi frequencies Ω_{12} and Ω_{23} describe the laser coupling (see sec. 2.1). We also performed the Rotating Wave Approximation [SZ97] here and transformed the Hamiltonian into a suitable interaction picture to eliminate an explicit time dependence of the Hamiltonian. Furthermore, we assumed the Rabi frequencies to be real.

In addition, the interaction between the Rydberg states has to be considered. In our case we use a pairwise interaction between all possible pairs. In [You09] it was shown that this is a valid assumption for most cases. A detailed discussion on the interaction can be found in chapter 3. Here we only note that typically the interaction is of the form of a van-der-Waals potential:

$$V_{ij} = \frac{C_6}{|\vec{R}_i - \vec{R}_j|^6} \tag{2.4}$$

This is a long-range interaction due to the large value of C_6 but goes to zero rapidly for large distances. Including the interaction, the total Hamiltonian then reads:

$$\begin{aligned} H &= \sum_i H^{(i)} + H_{\text{Int}} \\ &= \sum_i H^{(i)} + \hbar \sum_i \sum_{j>i} V_{ij} |rr\rangle^{(ij)(ij)} \langle rr| \end{aligned} \tag{2.5}$$

The coherent evolution of the density matrix is described by the von-Neumann equation:

$$\frac{d}{dt}\rho|_{\text{coh}} = -\frac{i}{\hbar}[H, \rho] \tag{2.6}$$

In principle, also the atomic movement would be a part of the Hamiltonian. As mentioned in section 1.1 though, experiments are typically carried out in the frozen Rydberg gas regime. In this cold regime the atoms hardly move on the timescale of the experiment and the contribution to the Hamiltonian can safely be neglected.

Now we include incoherent effects to the master equation. The most important is spontaneous emission from level a to level b for atom i. At zero temperature, which we are very close to, it reads [SZ97]:

$$\mathcal{L}_{\text{SE}}{}^{(i)}_{ab}[\rho] = -\frac{\gamma_{ab}}{2}\left(|a\rangle^{(i)(i)}\langle a|\rho + \rho|a\rangle^{(i)(i)}\langle a| - 2|b\rangle^{(i)(i)}\langle a|\rho|a\rangle^{(i)(i)}\langle b|\right) \tag{2.7}$$

The dephasing rates Γ_{ab} are included via:

$$\mathcal{L}_{\text{deph}}{}^{(i)}_{ab}[\rho] = -\frac{\Gamma_{ab}}{2}\left(|a\rangle^{(i)(i)}\langle a|\rho|b\rangle^{(i)(i)}\langle b| + |b\rangle^{(i)(i)}\langle b|\rho|a\rangle^{(i)(i)}\langle a|\right) \tag{2.8}$$

Their effect is that the off-diagonal elements in the density matrix, the coherences, are damped and decay.

Summing up all terms we arrive at the master equation:

$$\begin{aligned} \frac{d}{dt}\rho = &-\frac{i}{\hbar}[H, \rho] \\ &+ \sum_i \left(\mathcal{L}_{\text{SE}}{}^{(i)}_{32}[\rho] + \mathcal{L}_{\text{SE}}{}^{(i)}_{21}[\rho]\right) \\ &+ \sum_i \left(\mathcal{L}_{\text{deph}}{}^{(i)}_{32}[\rho] + \mathcal{L}_{\text{deph}}{}^{(i)}_{21}[\rho] + \mathcal{L}_{\text{deph}}{}^{(i)}_{31}[\rho]\right) \end{aligned} \tag{2.9}$$

2.3 Current State-of-the-Art Models

The full master equation from equation 2.9 would allow us to describe the system in a quite complete manner. However, the size of the density matrix grows exponentially

with the number of atoms. For N atoms and m states per atom the density matrix contains m^{2N} elements. To perform a naive full simulation for only 10 atoms with 3 states would require about 28 GB of storage for the density matrix. This example shows that one needs simplified models to treat a large number of atoms.

In the following we introduce some of the existing models. We start with a mean-field model which has been used with variations in several works [Ton04; Wei08; Cho08]. Then we explain the cluster expansion principle from [Sch10] and introduce the rate equation model from [Ate07a; Ate07b; ASP11]. For the sake of completeness we will also explain the basic principles for many-body Hamiltonian calculations which have been used in [RH05; You09], for example. However, we do not further analyse them in the scope of this work.

2.3.1 Mean-Field Models

The most simple models which arise from the master equation (eq. 2.9) are mean-field models. They have been used with some success to model early experiments [Ton04; Wei08; Cho08].

Different variations of mean-field models have been proposed but the main approximations are always the same. Here we limit our derivation to a single form. For simplicity, we restrict our discussion to the interaction part in the Hamiltonian. The other parts in the master equation do not couple different atoms and can be added later. We denote the reduced density matrix of the subsystem for atom i with $\rho^{(i)}$. It can be obtained by performing a trace over all other atoms:

$$\rho^{(i)} = \mathrm{Tr}_{\{1\ldots N\}\setminus\{i\}}\, \rho \tag{2.10}$$

Consequently, we denote the density matrix for two atoms i and j with $\rho^{(i,j)}$. In addition, we call the elements of the density matrix:

$$\rho^{(i)}_{ab} = {}^{(i)}\langle a| \cdot \rho^{(i)} \cdot |b\rangle^{(i)} \tag{2.11}$$

$$\begin{aligned}\rho^{(i,j)}_{ab,cd} &= {}^{(i)}\langle a| \cdot {}^{(j)}\langle c| \cdot \rho^{(i,j)} \cdot |b\rangle^{(i)} \cdot |d\rangle^{(j)} \\ &= {}^{(i,j)}\langle ac|\rho^{(i,j)}|bd\rangle^{(i,j)}\end{aligned} \tag{2.12}$$

Starting from equation 2.9 and tracing out all atoms but the atom i, we obtain the equation of motion:

$$\frac{d}{dt}\rho^{(i)}_{ab} = -i\sum_{j\neq i} V_{ij}(\delta_{ar} - \delta_{br})\rho^{(i,j)}_{ab,rr} \tag{2.13}$$

The equations for a single atom are coupled to two-atom density matrix elements. To obtain a closed set of only a few equations one truncates these elements in the mean-field models:

$$\rho^{(i,j)}_{ab,cd} \approx \rho^{(i)}_{ab} \cdot \rho^{(j)}_{cd} \tag{2.14}$$

This procedure is also called Hartree-Fock approximation [Bon98; Cho08]. With this simplification we now have $N \cdot m^2$ coupled equations, where m is the number of states.

Now we can exploit the fact that in an homogeneous setting each atom sees the same environment, to make the approximation:

$$\rho^{(i)} \approx \rho^{(j)} \tag{2.15}$$

With this assumption the number of equation decreases to only m^2. The sum over all interaction terms V_{ij} in equation 2.13 can be replaced by a suitable mean-field potential. However, it is not clear how the exact expression for this mean potential should look like and different techniques for its derivation were used [Ton04; Vog06b; Wei08; Cho08].

In this work we do not use the approximation from equation 2.15 and stick with a N atom description of the system. By this we avoid the problem of the ambiguity of the mean-field potential and have the possibility to perform spatially resolving simulations, for example.

2.3.2 Cluster Expansion

The cluster expansion for Rydberg atoms was used in [Sch10] to describe the dynamics of the Rydberg excitation.

While the mean-field models assume no correlations at all (eq. 2.14), this model also includes the two-atom density matrix elements $\rho^{(i,j)}$. The equations of motion for these elements read (again we neglect the non-interaction terms):

$$\begin{aligned}\frac{d}{dt}\rho^{(i,j)}_{a_ib_i,a_jb_j} =& -i\,V_{ij}(\delta_{a_ir}\delta_{a_jr}-\delta_{b_ir}\delta_{b_jr})\rho^{(i,j)}_{a_ib_i,a_jb_j}\\ &-i\sum_{k\neq i,j}V_{ik}(\delta_{a_ir}-\delta_{b_ir})\rho^{(i,j,k)}_{a_ib_i,a_jb_j,rr}\\ &-i\sum_{k\neq i,j}V_{jk}(\delta_{a_jr}-\delta_{b_jr})\rho^{(i,j,k)}_{a_ib_i,a_jb_j,rr}\end{aligned} \tag{2.16}$$

Again we have the so called hierarchy problem: the two-atom density matrix elements are coupled to three-atom density elements. In [Sch10] a truncation was suggested, which in principle is also applicable for even higher order truncation. The basic idea is to decompose the three-atom density matrix in different products of lower order density matrices. This procedure is known as cluster expansion [Bon98; Sch10]:

$$\rho^{(i,j)} = \rho^{(i)}\rho^{(j)} + g^{(i,j)} \tag{2.17}$$

$$\begin{aligned}\rho^{(i,j,k)} =& \rho^{(i)}\rho^{(j)}\rho^{(k)}\\ &+\rho^{(i)}g^{(j,k)}+\rho^{(j)}g^{(i,k)}+\rho^{(k)}g^{(i,j)}\\ &+g^{(i,j,k)}\end{aligned} \tag{2.18}$$

The correlations $g^{(i,j)}$ are not to be confused with the pair correlation function $g^{(2)}(r)$ (see sec. 7.3).

The next step in [Sch10] is to omit all contributions in 2.18 which describe large interactions between all three atoms at the same time. Therefore, we look at the terms in:

$$V_{ik}\,\rho^{(i,j,k)} = V_{ik}\left(\rho^{(i)}\rho^{(j)}\rho^{(k)}+\rho^{(i)}g^{(j,k)}+\rho^{(j)}g^{(i,k)}+\rho^{(k)}g^{(i,j)}+g^{(i,j,k)}\right) \tag{2.19}$$

It can be seen in equation 2.18 that the term $g^{(i,j,k)}$ obviously contains only three-atom correlations and becomes relevant only if all three atoms are close to each other. Hence, we neglect this term. In addition, the terms $V_{ik}g^{(j,k)}$ and $V_{ik}g^{(i,j)}$ only become large if atoms i and k are close to each other (otherwise V_{ik} would be small) and if atom j is close to atom k or i (otherwise the correlation g would be small). Thus, in order to have a contribution of these terms, all three atoms need to be close to each other and so we

neglect them, too. Note that the argument does not work for the term $V_{ik}g^{(i,k)}$. Now all terms which become only relevant in the cases where three or more atoms are close to each other were consistently dropped. Finally, we are left with:

$$\begin{aligned} V_{ik}\left(\rho^{(i,j,k)}\right) &\approx V_{ik}\left(\rho^{(i)}\rho^{(j)}\rho^{(k)} + \rho^{(j)}g^{(i,k)}\right) \\ &= V_{ik}\rho^{(j)}\rho^{(i,k)}, \end{aligned} \tag{2.20}$$

Note that these equations of motion with this approximation are consistent with respect to the single-atom equations: If we trace out atom i or atom j we retrieve the non-simplified expression of equation 2.13.

The simplifications made here are known as "ladder approximation" (LA) [Bon98]. However, if we only neglect the direct three-atom correlation $g^{(i,j,k)}$ and keep the rest of the terms, we end up with:

$$\rho^{(i,j,k)} = \rho^{(i)}\rho^{(j,k)} + \rho^{(j)}\rho^{(i,k)} + \rho^{(k)}\rho^{(i,j)} - 2\rho^{(i)}\rho^{(j)}\rho^{(k)} \tag{2.21}$$

This truncation of the density matrix corresponds to the "screened ladder approximation" (SLA) in [Bon98]. While the cluster expansion with LA can only describe situations where only one interaction energy is large for a given set of three atoms, the SLA contains all the necessary interaction terms and should also be able to describe systems at higher densities. Of course, still no three-body correlations are included in this model. The SLA can be seen as a high density addition to the cluster expansion model.

In the following we will mainly use the cluster expansion with LA, which is the model from [Sch10]. So we abbreviate this model simply with "cluster expansion". Whenever the SLA is used we note it explicitly.

2.3.3 Rate Equation

The rate equation model was introduced by Ates et al. [Ate07a; Ate07b]. The underlying equations are obtained from the master equation (eq. 2.9). The model relies on the fast damping of the single-atom coherences with respect to the excitation dynamics. In this case (and with $H_{\mathrm{Int}} = 0$ – for now we neglect the interaction) each atom can be described by a rate equation which in general looks like:

$$\dot{\sigma}_i = -a_{ii}\sigma_i + \sum_{j\neq i} a_{ij}\sigma_j \tag{2.22}$$

The coefficients a_{ij} are real numbers and the $\sigma_i = \rho_{ii}$ are the diagonal elements of the atom's density matrix, that means the probability that the atom is in the state i. The rate equation is obtained in the following way: By setting the time evolution of the coherences $\frac{d}{dt}\rho_{ij}$ to zero, one can solve for the coherences and get expressions for ρ_{ij}, which depend on the diagonal elements ρ_{ii}. These expressions can be used in the equations of motion for $\frac{d}{dt}\rho_{ii}$, which finally leads to coupled differential equations for the diagonals.

Note that the conservation of probability requires:

$$a_{ii} = \sum_{j\neq i} a_{ji} \tag{2.23}$$

The interaction from equation 2.5 can be included in an approximate way. The relevant part for atom i is:

$$\begin{aligned} H_{\text{Int}}^{(i)} &= \hbar \sum_{j \neq i} V_{ij} \cdot |rr\rangle^{(ij)(ij)} \langle rr| \\ &\approx \hbar \sum_{j \neq i} V_{ij} \cdot |r\rangle^{(i)(i)} \langle r| \cdot \rho_{rr}^{(j)} = \hbar \sum_{j \neq i} V_{ij} \cdot |r\rangle^{(i)(i)} \langle r| \cdot \sigma_r^{(j)} \end{aligned} \tag{2.24}$$

The expression was simplified here in order to include it in the rate equation system: Comparison with equation 2.3 shows that this expression has the same form as that of the laser detuning Δ_{23} and thus can be absorbed there. This effective detuning is dependent on the current state of all other atoms' $\sigma_r^{(j)}$, so that the equations of all atoms are coupled:

$$\Delta_{23,\text{eff}}^{(i)} = \Delta_{23}^{(i)} - \sum_{j \neq i} V_{ij}\, \sigma_r^{(j)} \tag{2.25}$$

The full system of equations still scales exponentially, but can be solved with Monte Carlo techniques if the coefficients a_{ii} are positive numbers. During a Monte Carlo simulation the variables σ_i become discret numbers zero and one, and the whole system jumps from one atomic configuration to the next. It is then easily possible to simulate several 1000 atoms in a short period of time. Note that in equation 2.25 the part $\sigma_r^{(j)}$ becomes zero or one in the Monte Carlo method, that means certain contributions of the interaction induced shift arise and vanish again in every Monte Carlo step. For a three-level-system (which is often used in an experiment) it is sometimes possible to introduce an effective ground state instead of the two non-Rydberg states. In this case, or if $m = 2$ anyway, the coefficients are indeed positive numbers.

In some cases one is also interested in the population of the intermediate state, e.g. when looking at EIT (see sec. 7.2). Then it is no longer possible to use the discussed rate equation, because for $m = 3$ the coefficients a_{ij} are partially negative and the Monte Carlo techniques do not work. Ates et al. recently suggested a method to overcome the negative coefficients [ASP11]. The basic idea is to use positive coefficients such that the steady state is not changed. The usual propagation can be written as:

$$\dot{\vec{\sigma}} = A \cdot \vec{\sigma} = \begin{pmatrix} -a_{11} & a_{12} & a_{13} \\ a_{21} & -a_{22} & a_{23} \\ a_{31} & a_{32} & -a_{33} \end{pmatrix} \cdot \begin{pmatrix} \sigma_1 \\ \sigma_2 \\ \sigma_3 \end{pmatrix} \tag{2.26}$$

Let now $\vec{\sigma}^{\text{SS}}$ be the steady state solution ($A \cdot \vec{\sigma}^{\text{SS}} = 0$). Then any other matrix B with positive coefficients and the property

$$B \cdot \vec{\sigma}^{\text{SS}} = 0 \tag{2.27}$$

can also be used to propagate $\vec{\sigma}$ to its steady state (just like with A in eq. 2.26, see also fig. 2.2). Of course we lose some physical information with this replacement. We can no longer obtain any information about the dynamics, only the steady state can be calculated. The condition of fast damping is also not necessary anymore, because in the steady state the relation $\dot{\rho}_{ij} = 0$ always holds for the coherences. The new trajectory of the matrix B has no physical meaning.

It is very important that the steady state is unique. If this was not the case, the new matrix could lead to a different steady state than the one determined by the initial

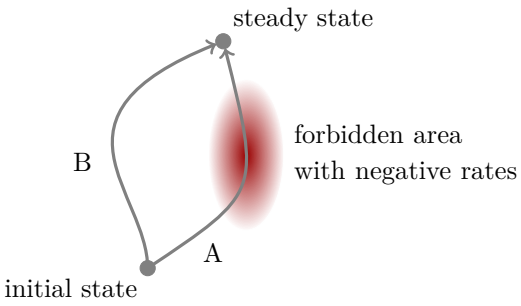

Figure 2.2: Alternative (non-physical) propagation into the steady state. The direct path is not accessible for Monte Carlo methods due to negative rates.

conditions and the physical trajectory. So in order to use this technique one also has to include a decay rate from the Rydberg level to the intermediate state in addition to [ASP11]. Otherwise the Rydberg state might decouple from the rest of the system at large detunings or large interaction energies, which would result in a subspace of the steady states with a dimension larger than one.

2.3.4 Many-Body Hamiltonian Calculations

In some cases it is possible to perform exact many-body calculations by solving the time dependent Schrödinger equation. The basic approach is to reduce the dimension of the Hilbert space by excluding certain states [RH05]. Usually it is growing like m^N where m is the number of states per atom and N is the number of atoms. If we implement the model on a computer, the requirement in CPU time limits the number of atoms which can be simulated. However, there are some cases where the calculation can be carried out for a higher number of atoms: Using special geometries and connected symmetries [OGL09], limiting the number of total excitations or using the blockade radius to discard multiple excited states [RH05; You09], one can reduce the number of states in the system and allow the calculation of about up to 100 atoms. Note that these models are dependent on certain geometries or high densities and are not suited in general. Moreover, they have the big disadvantage that they cannot be used for three-level systems as in fig. 2.1, because the truncation of the Hilbert space works only on the Rydberg states $|r\rangle$ and so an exponentially large number of states would remain. Another problem is that the Schrödinger equation does not include incoherent processes. Spontaneous emission could, for example, be included via a Monte Carlo technique [MCD93]. However, at high densities it is inevitable to use such models.

3 Rydberg-Rydberg Interaction

In this chapter we take a closer look at the interactions between Rydberg atoms in s-states. We begin with a simple picture which has been present in the literature for a while. Then we focus on the interaction in more detail and derive its spatial and radial dependence. This more detailed picture is then used to analyse if an incoherent decay is enhanced due to collective effects in the Rydberg system.

3.1 A Simple Picture

An intuitive image of the interaction between two Rydberg atoms can be found in [LTG05; You09] for example, or more detailed in [SWM10; CP10]. Here we follow the derivation of those publications.

Let a single atom be excited to the Rydberg state $|r\rangle$. Then two excited atoms would be in the product state $|rr\rangle = |r\rangle \otimes |r\rangle$. Rydberg states with slightly different principal quantum numbers n as well as different angular momentum quantum numbers l are close to each other with respect to their binding energy (sec. 1.2.1). If the energy gap between two different pair states such as $|ns, ns\rangle$ and $|np, (n\text{-}1)p\rangle$ is small or even zero, the dipole-dipole interaction leads to non-negligible coupling. These resonances are called Förster resonances [Vog06a]. So in general we have to include many states in the treatment of

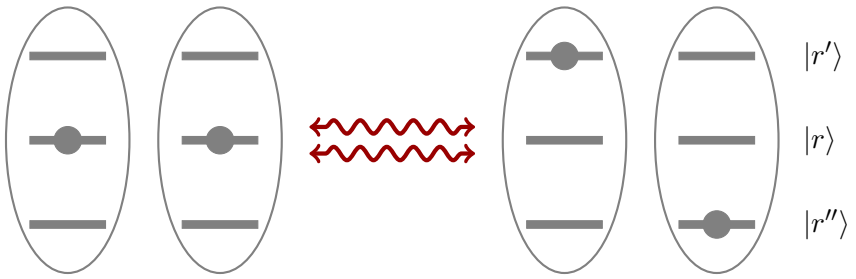

Figure 3.1: $|rr\rangle$ couples to other Rydberg pair states.

the interaction effect. For simplicity, we only look at two more Rydberg states: $|r'\rangle$ and $|r''\rangle$ (see fig. 3.1). Here the pair state $|rr\rangle$ is coupled to the state $|r'r''\rangle$ (as well to $|r''r'\rangle$, which we omit here). In this case the Hamiltonian reads:

$$H = \Delta|r'r''\rangle\langle r'r''| + \left(V^{dd}|rr\rangle\langle r'r''| + h.c.\right) \tag{3.1}$$

Here Δ denotes the energy difference between the doubly excited states $|rr\rangle$ and $|r'r''\rangle$. The coupling V^{dd} and the energy mismatch Δ are much larger than other typical parameters in the system. Therefore, we can diagonalize the subsystem of Rydberg states in a very good approximation. The eigenenergies are:

$$E_{\pm} = \frac{1}{2}\left(\Delta \pm \sqrt{\Delta^2 + 4|V^{dd}|^2}\right) \tag{3.2}$$

The dipole-dipole potential V^{dd} strongly depends on the interatomic distance. For typical experimental setups it is much smaller than the energy gap between the pair states ($|V^{dd}| \ll \Delta$). In this limit and with the assumption $\Delta > 0$ we arrive at the following eigenstates:

$$|-\rangle \approx |rr\rangle - \frac{V^{dd*}}{\Delta}|r'r''\rangle \tag{3.3}$$

$$|+\rangle \approx |r'r''\rangle + \frac{V^{dd}}{\Delta}|rr\rangle \tag{3.4}$$

We see that $|-\rangle$ is basically the unperturbed state $|rr\rangle$ and its coupling to non-Rydberg states (such as laser coupling in an experiment) is not changed. However, the change in energy can not be neglected:

$$E_- \approx -\frac{|V^{dd}|^2}{\Delta} \tag{3.5}$$

Since the dipole potential scales like $\frac{n^4}{R^3}$ and the level spacing like n^{-3} this interaction-induced energy shift can be written as:

$$E_- = -\frac{C_6}{R^6} \tag{3.6}$$

with

$$C_6 \sim n^{11} \tag{3.7}$$

This corresponds to a classical van-der-Waals interaction. In the case of Rydberg atoms ($n \gtrsim 30$) this energy can be very large and give rise to collective effects.

The eigenstate $|+\rangle$ is far off-resonant and hardly couples to the non-Rydberg states that $|-\rangle$ couples to. So it is save to neglect this state in our discussion. Note that if the condition $|V^{dd}| \ll \Delta$ is not fulfilled, the interaction becomes dipole-like ($\sim \frac{n^4}{R^3}$) and in general both eigenstates have to be considered.

In our discussion we only took into account one other pair state ($|r'r''\rangle$). In general the interaction energy for the state $|rr\rangle$ can be calculated with second order perturbation theory:

$$\Delta E^{(2)} = \sum_{\text{pair states i}} \frac{|V_i^{dd}|^2}{-\Delta_i} \tag{3.8}$$

3.2 A More Detailed Picture

The dipole coupling between atomic states can be derived from a fundamental level [Aga74; FS05; Kif10]. Quantizing the radiation field, coupling the field to the atoms and finally tracing out the field in an appropriate way gives (amongst others) a coherent coupling between two atoms:

$$\partial_t \rho = \ldots + i \sum_{i,j=1}^{D} \Omega_{ij} \left[S_{i+}^{(1)} S_{j-}^{(2)} + S_{j-}^{(1)} S_{i+}^{(2)}, \rho \right] \tag{3.9}$$

Here ρ is the density matrix for the two atoms and D denotes the number of dipole transitions. The operator $S_{i+}^{(n)}$ is defined as $|e_i\rangle^{(n)(n)}\langle g_i|$, where $|e_i\rangle^{(n)}$ is the excited and $|g_i\rangle^{(n)}$ the ground state of the i-th dipole transition of atom n. The coherent evolution of the density matrix is described with the von-Neumann equation (see eq. 2.6), thus the

terms $\Omega \cdot S^{(1)}S^{(2)}$ can be interpreted as an additional term in the system's Hamiltonian. For later use we abbreviate the expression for Ω_{ij}:

$$\Omega_{ij} = \frac{3}{2}\frac{\sqrt{\gamma_i\gamma_j}}{|\vec{d}_i||\vec{d}_j|}\left(\vec{d}_i\cdot\vec{d}_j^*\left(\left(\frac{1}{\eta}-\frac{1}{\eta^3}\right)\cos\eta-\frac{1}{\eta^2}\sin\eta\right)\right.$$
$$\left.-\frac{(\vec{d}_i\cdot\vec{R})(\vec{d}_j^*\cdot\vec{R})}{R^2}\left(\left(\frac{1}{\eta}-\frac{3}{\eta^3}\right)\cos\eta-\frac{3}{\eta^2}\sin\eta\right)\right) \tag{3.10}$$
$$= O_{ij}^{(1)}\cdot\vec{d}_i\cdot\vec{d}_j^* + O_{ij}^{(2)}\cdot\frac{(\vec{d}_i\cdot\vec{R})(\vec{d}_j^*\cdot\vec{R})}{R^2} \tag{3.11}$$

Here γ is the half-decay rate, $\vec{d}$ the dipole moment and $k = \eta/R$ is the wave vector of the corresponding dipole transition.

We consider the level structure of an atom which is shown in figure 3.2 and want to analyse the energy shift of the $|rr\rangle$ state. Note that pair states like $|14\rangle$ are energetically

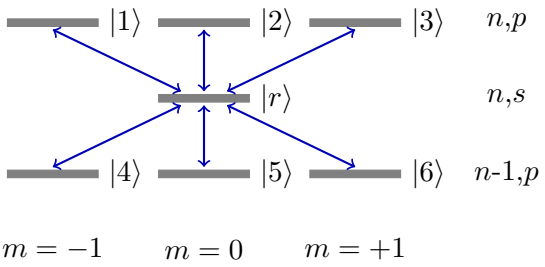

Figure 3.2: Level structure for one atom in an s-state with six dipole transitions to the adjacent p-states. The total subspace in m is considered.

close to $|rr\rangle$. Further, we assume degenerate energy levels with respect to m ($E_1 = E_2 = E_3, E_4 = E_5 = E_6$). For the given level scheme six different dipole transitions are possible: $|i\rangle \leftrightarrow |r\rangle$ $(1 \le i \le 6)$.

We are interested in the eigenstate (with respect to the coherent couplings Ω_{ij}), which is close to the unperturbed state $|rr\rangle$. It can be determined as:

$$|rr^*\rangle = \frac{1}{N}\left(c_{rr}|rr\rangle + \sum_{i=1}^{3}\sum_{j=4}^{6}\Omega_{ij}\left(|ij\rangle + |ji\rangle\right)\right) \tag{3.12}$$

with the definitions:

$$c_{rr} = \frac{\Delta}{2} + \frac{1}{2}\sqrt{\Delta^2 + 8\sum_{i=1}^{3}\sum_{j=4}^{6}|\Omega_{ij}|^2} \tag{3.13}$$
$$\Delta = 2E_r - E_1 - E_4 \tag{3.14}$$

The corresponding energy shift relative to $E_{rr} = 2E_r$ is:

$$\Delta_{rr^*} = E_{rr^*} - E_{rr} = -\frac{\Delta}{2} + \frac{1}{2}\sqrt{\Delta^2 + 8\sum_{i=1}^{3}\sum_{j=4}^{6}|\Omega_{ij}|^2} \tag{3.15}$$

All Ω appearing here represent a coupling between a (n-1),p and n,s state as well as a coupling between a n,p and n,s state. All variables in $O_{ij}^{(1)}$ and $O_{ij}^{(2)}$ are only dependent on the absolute values of the transition dipole moments $|\vec{d}|$ and the levels' energy differences ω. Since they appear in the same way for all Ω we can drop the indices i and j for simplicity.

In order to calculate the transition dipole moments

$$\begin{aligned} \vec{d_i} &= \langle i|e\vec{r}|r\rangle && (1 \leq i \leq 3) \\ \vec{d_i} &= \langle r|e\vec{r}|i\rangle && (4 \leq i \leq 6) \end{aligned}$$

we split the wave function in a radial and an angular part:

$$\Psi_{nlm}(r,\theta,\phi) = R_{nl}(r) \cdot Y_{lm}(\theta,\phi) \tag{3.16}$$

For $1 \leq i \leq 3$ we can then write:

$$\begin{aligned} \vec{d_i} = \langle i|e\vec{r}|r\rangle &= \int \Psi_{n1m_i}^* e\vec{r} \Psi_{n00} d^3r \\ &= e \int R_{n1} R_{n0} r^3 dr \cdot \int Y_{1m_i}^* \begin{pmatrix} \cos\phi \sin\theta \\ \sin\phi \sin\theta \\ \cos\theta \end{pmatrix} Y_{00} d\Omega \\ &= Q_1 \cdot \frac{\vec{n}_{m_i}}{\sqrt{3}} \end{aligned} \tag{3.17}$$

Similarly for $4 \leq i \leq 6$:

$$\begin{aligned} \vec{d_i} = \langle r|e\vec{r}|i\rangle &= \int \Psi_{n00}^* e\vec{r} \Psi_{(n-1)1m_i} d^3r \\ &= e \int R_{n0} R_{(n-1)1} r^3 dr \cdot \int Y_{00}^* \begin{pmatrix} \cos\phi \sin\theta \\ \sin\phi \sin\theta \\ \cos\theta \end{pmatrix} Y_{1m_i} d\Omega \\ &= Q_4 \cdot \frac{\vec{n}_{m_i}^*}{\sqrt{3}} \end{aligned} \tag{3.18}$$

The vectors $\vec{n}$ satisfy the relation $\vec{n}_i^{\mathrm{T}} \cdot \vec{n}_j^* = \delta_{ij}$ as well as $\sum_i \vec{n}_i^* \cdot \vec{n}_i^{\mathrm{T}} = \mathbb{1}$.

Now we can calculate the sum which appears in the expression for the energy shift:

$$\begin{aligned} \sum_{i=1}^{3}\sum_{j=4}^{6} |\Omega_{ij}|^2 &= \sum_{i=1}^{3}\sum_{j=4}^{6} |O^{(1)} \frac{Q_1 Q_4}{3} \delta_{m_i m_j} + O^{(2)} \frac{Q_1 Q_4}{3} \frac{(\vec{n}_{m_i} \cdot \vec{R})(\vec{n}_{m_j}^* \cdot \vec{R})}{R^2}|^2 \\ &= \frac{(Q_1 Q_4)^2}{9} \left(3{O^{(1)}}^2 + 2O^{(1)}O^{(2)} + {O^{(2)}}^2 \right) \end{aligned} \tag{3.19}$$

Note that all vectors and directions have vanished. The interaction energy is therefore independent of the atoms' orientation as one would expect for an s-state. For different angular quantum numbers this is not the case, as nicely reported in [Car04].

The final form for the energy shift is ($\eta = k_0 R$):

$$\begin{aligned} \Delta_{rr^*} = \frac{1}{2}\Big(&- \Delta + \\ &\sqrt{\Delta^2 + 18\frac{\gamma_1\gamma_4}{\eta^6}\left(3 + \eta^2 + \eta^4 + (3 - 5\eta^2 + \eta^4)\cos(2\eta) - 2\eta(\eta^2 - 3)\sin(2\eta)\right)}\Big) \end{aligned} \tag{3.20}$$

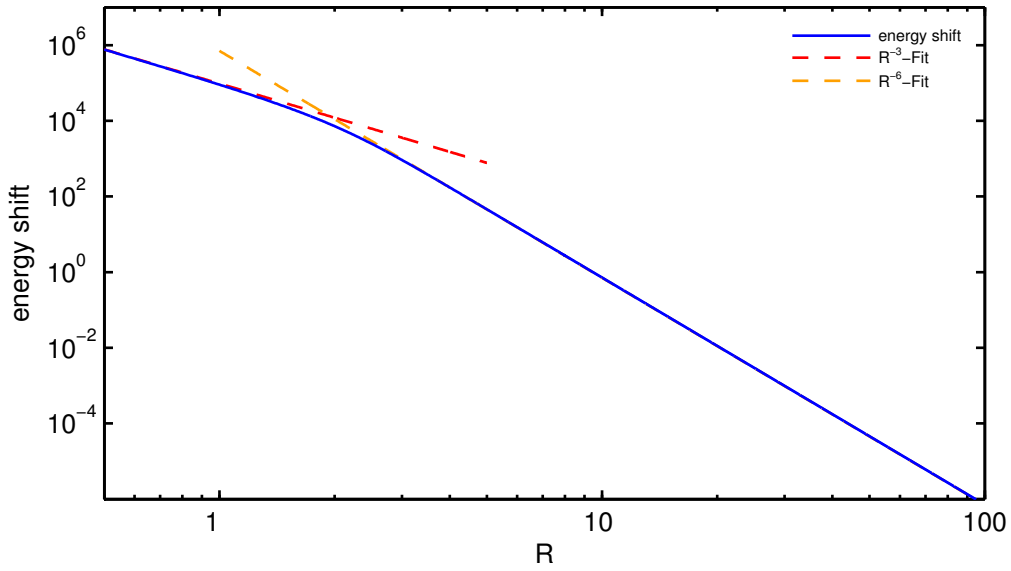

Figure 3.3: Energy shift of the doubly excited Rydberg state (eq. 3.20) for Rb, n=61.

For small distances (small η) the shift behaves like R^{-3}, for intermediate distances like R^{-6} (cf. eq. 3.6). This can be seen in figure 3.3 where the interaction shift is plotted for Rubidium atoms excited to $n = 61$. The transition dipole moments were calculated with the expressions given in [CP10] and the energies were taken from [Li03]. The $1/R$ and $1/R^2$ expressions for the retarded dipole-dipole interaction in Ω only become important at larger distances where $\eta = k_0 R \approx 1$, while in our case $\eta \ll 1$. We conclude that retarded potentials are not relevant for our system.

Note that the expression 3.20 is not the total energy shift which is observed in an experiment. We derived this formula for a limited number of states per atom. In general more of these states, and thus pair states, have to be considered.

In the following we always assume densities for which the interaction energy behaves like $V = C_6 \cdot R^{-6}$. With the system of units from section 2.1 the coefficient C_6 is given in units of MHz $\cdot\, \mu$m^6. Numerical values for C_6 can be found in [Sin05], for example.

3.3 Incoherent Coupling

The collective states $\frac{1}{\sqrt{2}}(|ge\rangle \pm |eg\rangle)$ in a two-level system are super- and subradiant, respectively [Aga74; FS05; Kif10]. It is therefore of interest, if the decay of the state $|rr^*\rangle$ also shows collective behaviour. In our case we have a seven-level system and the simple pictures from two-level atoms cannot generally be applied directly. Again we want to tackle the problem from a fundamental level.

Aside from the coherent coupling (eq. 3.9), incoherent processes can be a part of the master equation. Here we want to focus on the collective decay which for two atoms is

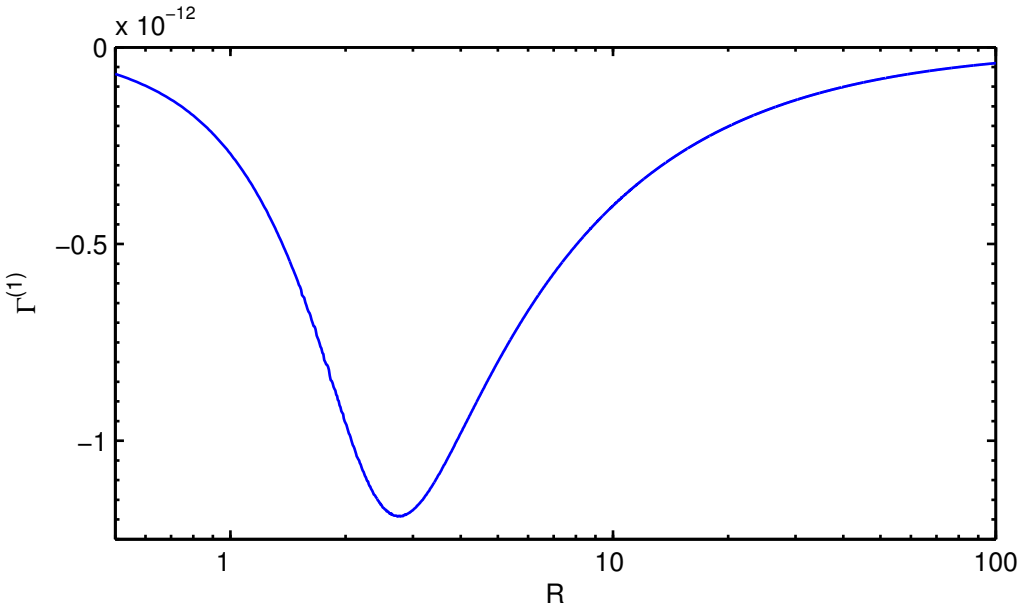

Figure 3.4: Collective decay rate of the doubly excited Rydberg state in frist order (eq. 3.22) for Rb, n=61.

given by [Aga74; FS05; Kif10]:

$$\partial_t \rho = \ldots - \sum_{i,j=1}^{D} \Gamma_{ij} \left(\left(S_{i+}^{(1)} S_{j-}^{(2)} + S_{j-}^{(1)} S_{i+}^{(2)} \right) \rho + \rho \left(S_{i+}^{(1)} S_{j-}^{(2)} + S_{j-}^{(1)} S_{i+}^{(2)} \right) \right.$$
$$\left. -2 S_{j-}^{(2)} \rho S_{i+}^{(1)} - 2 S_{j-}^{(1)} \rho S_{i+}^{(2)} \right) \quad (3.21)$$

To check if this process is important for our terms we calculate the dynamics of the state $|rr^*\rangle$ in first order, where $|rr^*\rangle$ is the eigenstate from equation 3.12. We find:

$$\begin{aligned} \Gamma^{(1)} &= \langle rr^* | \dot{\rho} | rr^* \rangle \big|_{\rho = |rr^*\rangle\langle rr^*|} \\ &= -\frac{4 c_{rr}}{N^2} \left(c_{rr}^2 + 2 \sum_{i=1}^{3} \sum_{j=4}^{6} |\Omega_{ij}|^2 \right) \left(2 \sum_{i=1}^{3} \sum_{j=4}^{6} \Re(\Omega_{ij}^* \Gamma_{ij}) \right) \end{aligned} \quad (3.22)$$

A similar calculation as in the coherent case can be performed which finally leads to a orientation independent expression. Here we only give the limit for small η:

$$\Gamma^{(1)} = -\frac{22}{5} \sqrt{\frac{\gamma_1 \gamma_4}{3}} \eta^2 + \mathcal{O}(\eta^4) \quad (3.23)$$

The obtained rate for the collective decay in first order is plotted in figure 3.4. As one can see this effect is totally negligible due to its order of magnitude. Interestingly, it is pronounced at about $3\,\mu m$. However, its effect is way too small to be seen in any experiment. We remark that our analytic calculation was performed in first order and thus it is only valid for small timescales.

In [Wan07] and [DBW08] superradiant effects in Rydberg atoms were reported, though. Apparently, a higher order calculation of the collective decay would be required to reproduce this effect. However, a fully analytical treatment is impractical in our considered system.

4 Speed Improvements

Right next to the physical capabilities of a model it is also of decisive importance how fast it can simulate a given setup or give new predictions.

In this chapter we describe methods which allowed us to speed up some existing models considerably.

4.1 Rate Equation

The rate equation is generally a fast technique because it can be solved with Monte Carlo algorithms and so is not dependent on time consuming integration. An overview on suitable algorithms for Rydberg systems is given in [Cho08]. However, as we have seen in section 2.3.3, it is sometimes necessary to omit the physical trajectory and only calculate the system's steady state. In these cases, for instance for a general three-level system, the Monte Carlo procedure can be reduced and we can improve the runtime of the rate equation.

While the new matrix B in the rate equation (sec. 2.3.3) is of the type $A + \Delta A$ in [ASP11], it is even easier if we construct an entirely new matrix. The correction matrix ΔA has the disadvantage that it is different for every set of parameters and a general solution would be convenient. Let $\vec{\sigma}^{\mathrm{SS}}$ be the steady state solution of a single atom without interaction. It is either known or very easy to compute numerically in contrast to the N-atom solution. Thus, the probabilities σ_i^{SS} can be used for B:

$$B \sim \begin{pmatrix} \sigma_1^{\mathrm{SS}} - 1 & \sigma_1^{\mathrm{SS}} & \sigma_1^{\mathrm{SS}} \\ \sigma_2^{\mathrm{SS}} & \sigma_2^{\mathrm{SS}} - 1 & \sigma_2^{\mathrm{SS}} \\ \sigma_3^{\mathrm{SS}} & \sigma_3^{\mathrm{SS}} & \sigma_3^{\mathrm{SS}} - 1 \end{pmatrix} \tag{4.1}$$

Note that the so constructed matrix naturally fulfills the relations 2.23 and 2.27.

Since we already gave up the knowledge of the exact dynamical processes we can neglect every time occurrence in the Monte Carlo method. In [Cho08] the Kinetic Monte Carlo (KMC) algorithm was suggested for the integration of a rate equation where one has information about the dynamics (e.g. for $m = 2$). In some parts of the literature the algorithm is called Variable Size Step Method (VSSM), while KMC is slightly different [Jan03]. KMC uses a variable time step, based on the current jump probabilities. However, the time information is irrelevant for our purpose. Instead, we use a modification based on the Random Selection Method (RSM, cf. [Cho08; Jan03]). Schematically, the calculation procedure is as follows:

1. Set atom i to state m_i, e.g. $m_i = 1$ for ground state
2. Pick random atom j
3. Calculate steady state σ_k^{SS} $(1 \leq k \leq m)$ for atom j, based on current configuration of all other atoms
4. Pick random number $r \in [0, 1)$
5. Change atom j's state to state l, where l is the largest integer with $\sum_{k=1}^{l-1} \sigma_k^{\mathrm{SS}} < r$
6. Go back to step 2 until a steady state criterion is fulfilled

It is more intuitive to think of an iterative approximation to the many-body steady state.

4.1.1 Convergence

Now we have to find a condition when the Monte Carlo algorithm is to be stopped. We let the Monte Carlo simulation perform a variable number of steps for a certain set of parameters. We note that the obtained result is averaged over many runs and many geometric realizations. As seen in fig. 4.1, the observable ρ_{rr}, which is the probability to

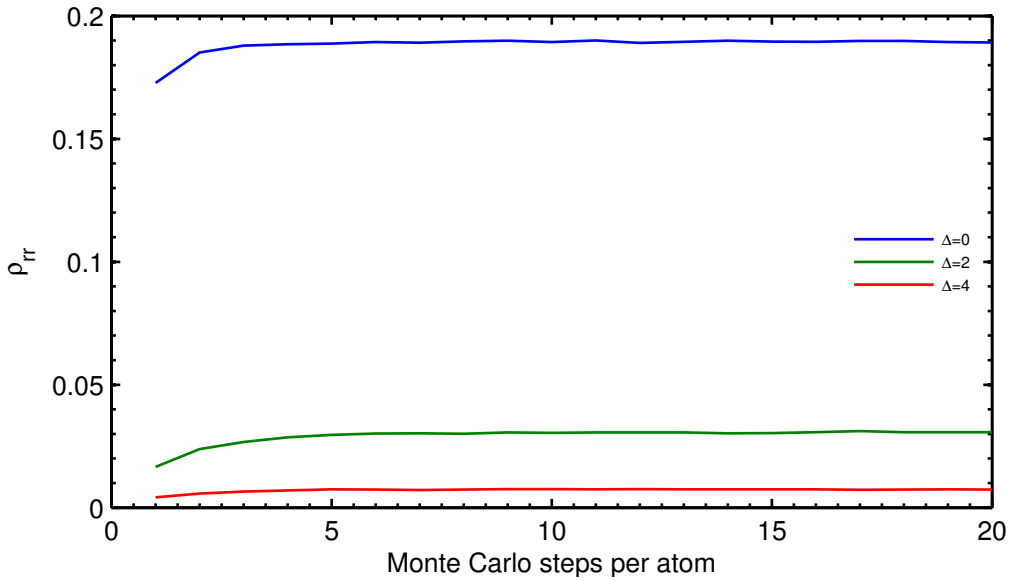

Figure 4.1: Convergence of the Monte Carlo method. Parameters: $\Omega_{12} = 2, \Omega_{23} = 1$, $\gamma_{21} = 6, \gamma_{32} = 1/40, \Gamma_{32} = \Gamma_{21} = 0.1, C_6 = 900/2\pi, N = 500, n_{1\mathrm{D}} = 1$.

find an atom in the Rydberg state, reaches its final value after $\approx 7 \cdot N$ steps, independent of the chosen laser detuning. In the following we will always run the simulation with $10 \cdot N$ steps to make sure that the system is indeed in the steady state.

4.1.2 Fast Calculation of the Steady State

The key to the use of the faster rate equation model is the fast calculation of an atom's steady state. Usually several thousand Monte Carlo runs are needed, each with $\approx 10 \cdot N$ steps (sec. 4.1.1). In each step a steady state has to be calculated. Moreover, as we will see in the next chapter, it is also important to calculate the steady state of a larger system than of a single atom. Therefore, it is necessary to speed up this computation.

The master equation (eq. 2.9) for a single atom or a pair of atoms is linear and can thus be written in the form:

$$\dot{\vec{\rho}} = M \cdot \vec{\rho}, \tag{4.2}$$

where $\vec{\rho}$ contains all elements of the density matrix in one column. The problem to find the steady state is then equivalent of finding the eigenvector of M with eigenvalue zero. Note that M is not invertible because of the probability conservation $\sum_i \rho_{ii} = 1$. Thus, a non-trivial solution for the eigenvector, the steady state, exists. For our purpose the steady state is always unique (all states are coupled). The matrix M can be decomposed into a product of a unitary matrix Q and an upper triangular matrix R (QR decomposition, [SK11]):

$$M = Q \cdot R \tag{4.3}$$

Since M is not of full rank, neither is R. This means that the element in the last column and last line of R vanishes. It is then possible to create the eigenvector by back substitution. Since we are only interested in the elements ρ_{ii} and not ρ_{ij} in general, it is useful to arrange the elements in $\vec{\rho}$ such that the elements ρ_{ii} are located at the back of the vector $\vec{\rho}$. Then the back substitution is faster.

By using the real and imaginary parts of the coherences separately we can transform $\vec{\rho}$ and M into a real vector and a real matrix, respectively. To reduce the number of variables in $\vec{\rho}$, and thus the matrix' size, one can use the fact that the density matrix is Hermitian: $\rho_{ij} = \rho^*_{ji}$.

The QR decomposition can be implemented in different ways. The methods using Householder transformations and Givens rotations are stable algorithms [SK11] and should be preferred. Since the matrix M is sparse, an algorithm which uses Givens rotations is usually better [SK11].

We compared the speed of the steady state computation for different algorithms, such as QR and Singular Value Decomposition (SVD, [SK11]) and direct eigenvector calculations. For our purposes it turned out that the QR distribution combined with Givens rotations is the fastest way to obtain the steady state of a system. An exception is the two-level case of a single atom: Here, the explicit analytic formulas for the steady state values are simple in their structure, which makes the direct computation faster than a numerical calculation.

4.1.3 Computation of Observables

In a single Monte Carlo run one obtains a discrete atom configuration in the sense that each atom is either in state $|g\rangle$, $|m\rangle$ or $|r\rangle$, but not in a superposition.

Let us first consider the case of a $g^{(1)}$-type observable $\langle\mathcal{O}\rangle$. Here $\mathcal{O}$ is a operator which can be written as a sum of operators, which all act only on a single atom. In other words, $\mathcal{O}$ does not take into account correlations between atoms. Such an observables is, for instance, the excitation probability of a certain state. It can be calculated by dividing the number of atoms in that state by the total number of atoms. However, this value often fluctuates strongly around its mean and it takes many Monte Carlo runs to obtain a smooth curve. For such a type of observable it is possible to lower the number of needed Monte Carlo runs with the following technique: After each Monte Carlo run we have a certain atomic configuration. Based on this, we can again calculate every atom's steady state. The result for each atom now is not a quantum mechanical superposition, but a partition of the atomic states: σ_g, σ_m and σ_r (with the sum being 1). When we use these σ to calculate the observable, the resulting curves become smooth much faster.

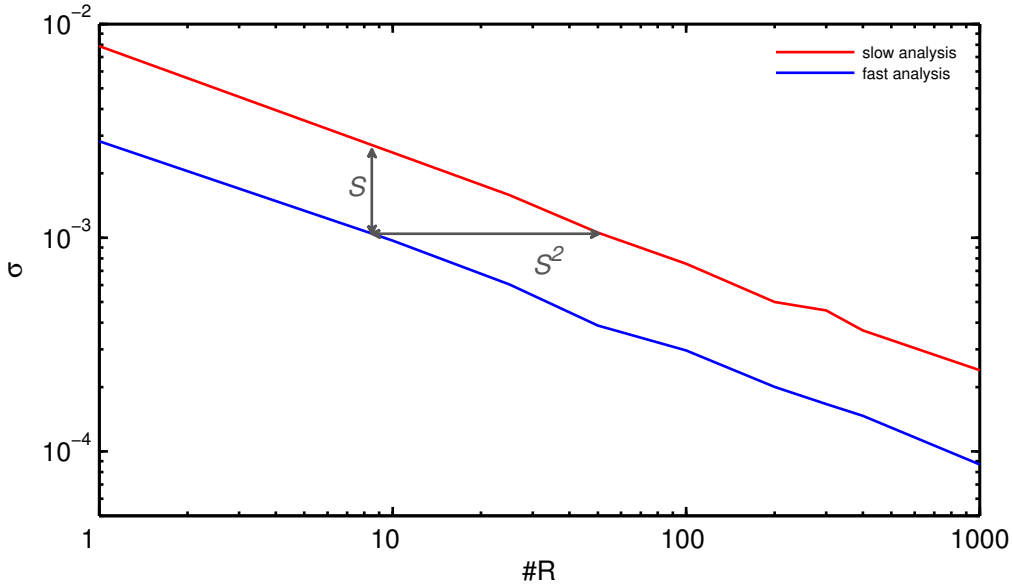

Figure 4.2: Smoothness of a curve obtained by two different evalution schemes. The deviation from the limit of infinitely many Monte Carlo runs $\#R \to \infty$ (eq. 4.6) is shown. Parameters: $\Omega_{12} = 2, \Omega_{23} = 1, \gamma_{21} = 6, \gamma_{32} = 1/40$, $\Gamma_{32} = \Gamma_{21} = 0.1, C_6 = 310000/2\pi, N = 500, n_{1D} = 1$. The data points x_i are taken from $\rho_{rr}(\Delta_{23})$ at $-7 \leq \Delta_{23} \leq 7$.

Let us consider the calculation of the Rydberg excitation probability after a single Monte Carlo run, for example. The slow way is to count all Rydberg atoms and to divide them by the total number of atoms:

$$\rho_{rr}^{(\text{slow})} = \frac{N_R}{N} \tag{4.4}$$

The faster method is to calculate each atom's probability $\sigma_r^{(i)}$:

$$\rho_{rr}^{(\text{fast})} = \frac{\sum_{i=1}^{N} \sigma_r^{(i)}}{N} \tag{4.5}$$

To quantify the speedup, we define the quantity σ, which indicates the deviation to the curve obtained in the limit of infinitely many runs:

$$\sigma = \sqrt{\frac{1}{p-1} \sum_{i=1}^{p} (x_i - x_i^{(0)})^2} \tag{4.6}$$

Here p is the number of data points on the curve and $x_i^{(0)}$ are the reference values. This quantity σ was averaged over 25 different spatial realizations and plotted over the number of Monte Carlo runs $\#R$ in figure 4.2. It is clearly visible that the second technique has a smaller deviation σ and produces the same result in the limit of many runs, since both lines approach zero and the same reference values $x_i^{(0)}$ were used. For both methods σ is proportional to the inverse square root of the number of simulations. Moreover, if we run the analysis with different atom numbers N, we find:

$$\sigma \sim \frac{1}{\sqrt{N \cdot \#R}} \tag{4.7}$$

For the case plotted in figure 4.2 we see that $S = \frac{\sigma^{(\text{slow})}}{\sigma^{(\text{fast})}} \approx 2.8$. This means, to gain the same smoothness with both methods, the fast one needs $S^2 \approx 2.8^2 \approx 7.8$ times less Monte Carlo runs. This amplifies even further if we look at the curve $\rho_{mm}(\Delta_{23})$. Here S becomes ≈ 38. We record that the second method, which uses one more steady state calculation for every atom, needs, of course, some more time, but gives way less fluctuations and therefore is to be preferred.

The second kind of observables $\langle \mathcal{O} \rangle$ with operator $\mathcal{O}$ cannot be written as a sum of operators acting on single atoms. Examples are the Mandel Q parameter or the pair correlation function $g^{(2)}$ (see sec. 7.3 and 7.4). In these cases it is not possible to speed up the data analysis, since the trick with another steady state calculation does not include possible long range correlations. The data, for instance the number of excited pairs with distance R, has to be counted explicitly from the atomic configuration right after all Monte Carlo steps.

4.2 Cluster Expansion

In contrast to the rate equation, the cluster expansion (see sec. 2.3.2) is not a Monte Carlo based model but depends on integration of differential equations. To make the computation more efficient we can use different methods.

The most effective improvement is to reduce the dimension of the system of differential equations. For $m = 3$ states per atom, the density matrix for two atoms contains $3^4 = 81$ independent variables. Since we have $\binom{N}{2} = \frac{N}{2}(N-1)$ pairs in our system, the number of differential equations is $81 \cdot \frac{N}{2}(N-1)$. The large prefactor in the scaling limits the number of atoms which we can simulate with this model. A good ansatz is to limit the number of pairs in our system. It seems obvious, that atoms with a very large distance are not correlated anymore. We can include this idea if we introduce a critical distance L_{Cr}: for each two atoms, whose distance is smaller than L_{Cr}, a pair is included in the simulation, otherwise we use the approximation 2.14: $\rho^{(i,j)} \approx \rho^{(i)}\rho^{(j)}$. This critical distance has to be chosen adequately: It can be seen in the pair correlation function that starting from a certain distance this relation 2.14 holds (see sec. 7.3). Of course, the value for L_{Cr} depends on the parameters in the system. In practice, this distance can be chosen larger without changing the results, but this means more pairs in addition and thus a larger runtime.

Using this improvement, the number of pairs N_{Pairs} only scales linearly. Leaving out finite size effects, we can estimate for a 3-d random sample:

$$N_{\text{Pairs}} \approx \frac{1}{2} \cdot N \cdot (\frac{4\pi}{3} L_{Cr}^3 \, n_{3\text{D}}) \tag{4.8}$$

For very high densities and a fixed value of L_{Cr}, the number of pairs will approach the maximum number $\frac{N}{2}(N-1)$. However, these densities are not in the validity range of the model, because then more than exact two-atom correlations should be included.

With this method the dimension of our systems now does not scale strictly with $\mathcal{O}(N^2)$, but with $\mathcal{O}(N)$ and a density dependent prefactor.

The second technique we use to improve the runtime is to reduce the number of calculations of all derivatives in the differential equation system. A problem which often

occurs are large interaction terms in contrast to the rather small parameters such as the laser couplings. Then the system of differential equations becomes "stiff" and conventional algorithms need very small time steps to solve the system accurately [SK11]. Therefore, we set an upper limit for the interaction strength. We reduced this limit successively from $\approx 10^9$ to lower numbers to make sure the results of the simulations are not affected by this. To ensure that this limit is certainly not changing the physics we use a minimal upper limit which is two orders of magnitude higher than any other parameter in the system. Using this method we can reduce the stiffness of the system considerably and speed up the calculation substantially.

The last approach for a general speed up can be done for the calculation of the derivatives. These derivatives have to be calculated in every time step. Looking at the equations of motion (eq. 2.16) we note that the most time consuming part is the calculation of terms of the form $\sum_{k\neq i,j} V_{ik}\rho^{(j)}_{\cdot\cdot}\rho^{(i,k)}_{\cdot\cdot,rr}$. For the worst case with $\mathcal{O}(N^2)$ pairs in the system, the calculation has a scaling of $\mathcal{O}(N^3)$. However, it is possible to create a table in advance where we calculate $\sum_{k\neq i} V_{ik}\rho^{(i,k)}_{\cdot\cdot,rr}$ for every atom i, which only takes a time of $\mathcal{O}(N^2)$. This table can be used to compute all the required terms directly.

With these three modifications the simulation runs considerably faster than a straightforward implementation. Note, however, that the cluster expansion with SLA cannot benefit from a table which is constructed in advance: Next to the above mentioned sum, several other contributions add to the equations of motion and not all of them can be constructed with the help of an $\mathcal{O}(N^2)$ table.

5 The Hybrid Model

One of the major limitations in the rate equation model is the interaction which is only included approximately (eq. 2.24): The interaction induced energy shift is included in an effective laser detuning and not as an exact two-particle effect. In fig. 5.1 we plotted

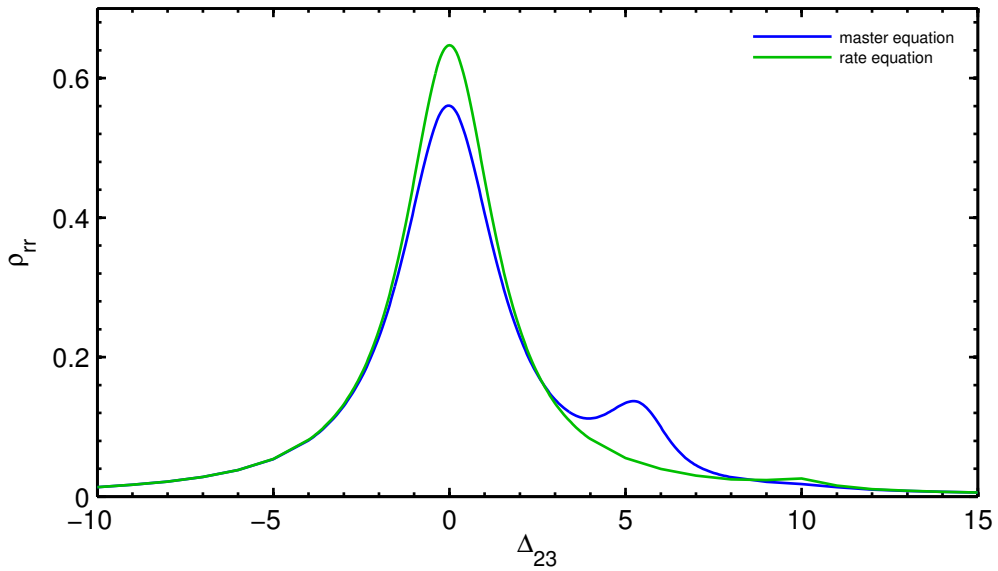

Figure 5.1: Deviation of the rate equation from the master equation (N=2). Parameters: $\Omega_{12} = 3, \Omega_{23} = 3, \gamma_{21} = 6, \gamma_{32} = 1/40, V_{12} = 10$.

the Rydberg excitation ρ_{rr} against the upper laser detuning Δ. We considered only two atoms here, because then the exact solution of the master equation can be calculated easily.

Obviously, the two curves do not agree very well. For example, the master equation predicts a second resonance at $V/2$, which can be understood as a 2-photon-process: For $\Delta = 0$ the transition $|mm\rangle \leftrightarrow |rr\rangle$ is off-resonant by $V - 2\Delta = V$. In the case of $\Delta = V/2$ the excitation path is resonant and appears in the image. The maximum is not exactly at $\Delta = V/2$ which is presumably caused by the presence of the level $|g\rangle$ and Autler-Townes-like shifts. The rate equation does not take into account this 2-γ-process at all, because the corresponding terms were dropped when the interaction was included. In principle, one could heuristically introduce a new rate which quantifies the transition $|mm\rangle \leftrightarrow |rr\rangle$, but we develop a better technique in the next section.

5.1 Derivation

Let us consider two atoms which interact with some potential V_{12}. Instead of three levels, our system now has $3^2 = 9$ levels and its density matrix consists of $3^4 = 81$ elements.

The master equation looks like:

$$\frac{d}{dt}\rho = -\frac{i}{\hbar}\left[H^{(1)} + H^{(2)} + \hbar\, V_{12}|rr\rangle\langle rr|, \rho\right] + \text{incoherent terms} \tag{5.1}$$

For a given set of parameters it is still possible to calculate the system's steady state numerically (see sec. 4.1.2). We are interested in the steady state values of the levels' population probabilities, for example $\rho_{gg,mm}$, which is the probability of the first atom to be in state $|g\rangle$ and the second atom to be in $|m\rangle$. We can construct a similar matrix as in eq. 4.1. Instead of a 3×3-matrix, the matrix' size is 9×9. Integrating the equation

$$\dot{\vec{\sigma}} = B \cdot \vec{\sigma} \tag{5.2}$$

or solving the system with a Monte Carlo algorithm would give the two atoms' steady state again. Note that this steady state is exact for the two atoms, because we took into account the full interaction in equation 5.1 and not just a simplified expression as in the rate equation case (eq. 2.24). During the Monte Carlo run not only a single atom can change its state per step, but also both atoms at the same time, for instance $|mr\rangle \to |rg\rangle$. Single atom jumps are included naturally: $|ac\rangle \to |bc\rangle$.

Now we derived a method to calculate a pair's steady state with a Monte Carlo technique. At this point the calculation is unnecessary, because the steady state has to be known in the first place to construct the matrix B. It is needed, however, if we expand this ansatz to a higher number of atoms.

5.1.1 Three Atoms

While the exact solution of the master equation (eq. 2.9) is still possible for three atoms, we now try to find an alternative way based on the one- and two-atom steady states, which then also can be expanded to even higher atom numbers.

We look at the following setup: The atoms 1 and 2 are placed such that the potential V_{12} is rather large. The third atom is moved towards the pair from $R \to \infty$ until the three atoms form an equilateral triangle. At the same time the interaction strength $V_{13} = V_{23}$ increases from 0 to V_{12}. We test three models that are based on single- or two-atom steady states. As a benchmark we compute the Rydberg excitation probability for different interaction strength $V_{13} = V_{23}$ and detuning Δ_{23}. Finally, we determine the deviation from the exact solution (eq. 2.9 with $N = 3$). Our simplified models are:

(a) We use the method which we described in section 4.1. During the Monte Carlo simulation an atom is randomly chosen, its steady state is calculated (based on the current atomic configuration), and performs a jump. At no point the exact interaction between a pair of atoms is considered, the potentials are absorbed in the effective detuning.

(b) Out of three atoms one can create three different pairs of atoms. During the simulation one of these pairs is chosen, its steady state is calculated and the pair's state is changed. The interaction between the pair's atoms is implemented exactly, while the interaction with the third atom is included in the effective detuning.

(c) Since most of the time only the first two atoms are very close together, we only use this pair. The interaction of these two atoms is used exactly. The third atom is always handled with a single atom method (just as in (a)).

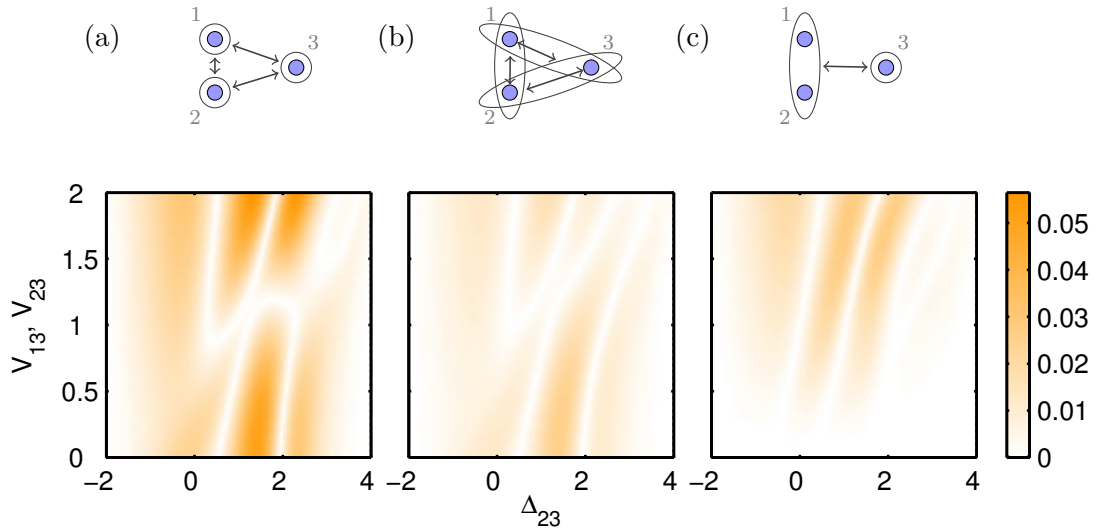

Figure 5.2: Deviation $|\rho_{rr}^{\text{simpl.}} - \rho_{rr}^{\text{exact}}|$ from the simplified models (a), (b) and (c) to the exact solution (master equation) for $N = 3$. Parameters: $\Omega_{12} = 3$, $\Omega_{23} = 2$, $\gamma_{21} = 6$ and $\gamma_{32} = 1/40$.

The result of the comparison is shown in figure 5.2.

Method (a) shows strong deviations over a large range of interactions and detunings. Except from the part where $\Delta_{23} \approx 0$, the differences arise from special three-atom resonances. In none of the models these resonances can be reproduced, because then all interaction terms would have to be included.

The second model shows a good precision over all ranges, but surprisingly fails at the "easy" situation, where $V_{13} = V_{23} = 0$. This can be explained by the fact that the pairs overlap. With this we mean that a single atom is part of two or even more different pairs. When we look at the first atom it is treated exactly if it is paired with the second atom. If it is paired with the third one, then the interaction effect which comes from atom 2 is only included in the effective detuning. Thus, the result of the first atom's behaviour is a mix of the exact and the inexact treatment. We note that such overlapping pairs should be avoided in this limit. In addition, a larger number of pairs also slows down the runtime of the simulation.

In the case where the second model fails, the third model (c) performs very well. For $V_{13} = V_{23} = 0$ the model is exact, because the third atom can be separated in a mathematical sense ($\rho^{(1,2,3)} = \rho^{(1,2)} \cdot \rho^{(3)}$), which corresponds to the procedure of not including pairs containing atom 3 in the model.

To obtain a good precision over all ranges, we have to combine the models (b) and (c). As we have seen, model (c) works well for small potentials, model (b) rather well for large potentials. Therefore, we can define a critical interaction strength V_{Cr} (or a critical distance R_{Cr} with $\frac{C_6}{R_{Cr}^6} = V_{Cr}$) that determines when which model has to be used (see fig. 5.3). Note that when we switch between these two models during the computation of some observable, for example $\rho_{rr}(V_{13})$, the resulting curve is not continuous in general.

Summing up: The combination of models (b) and (c) gives the most precise solution for three atoms out of the simplified models which were considered here. It gives a very good solution if one atom is very far apart from two other atoms. In the case where all

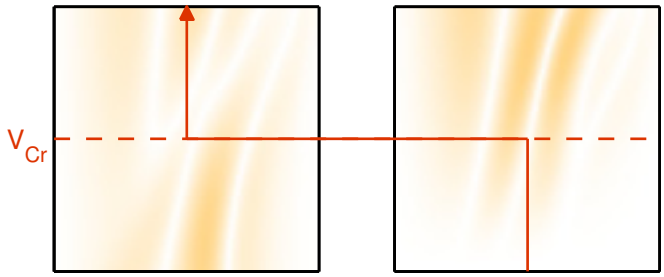

Figure 5.3: Models (b) and (c) are to be used for the best result, V_{Cr} defines the crossover.

atoms are close to each other, the method shows deviations, but gives a better solution than the rate equation (model (a)).

5.1.2 *N* Atoms

Now that we found a relatively precise model for three atoms based on one- and two-atom calculations, it is a straightforward process to expand this model to higher atom numbers. From three atoms we learned that we should use a pair description for atoms with large interactions. On the other hand, these pairs must not overlap a lot, since then pair information is destroyed again. Therefore, we keep the concept of a critical

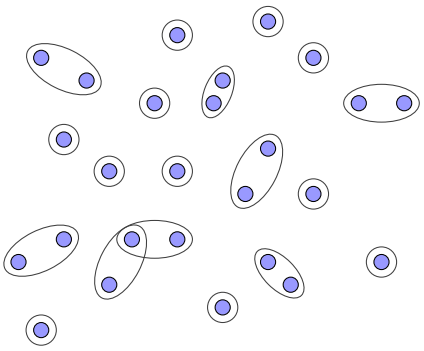

Figure 5.4: N atoms divided into pairs and single atoms.

interaction (or equivalent: a critical distance), which allows us to divide all atoms in either pairs or single atoms. Since we use a mixture of a one- and two-atom description, we call this the Hybrid model.

The order of magnitude of the critical distance R_{Cr} can be assigned with the help of the next neighbour distance R_{NN}. The calculation of R_{NN} from [Amt08] can easily be performed in any dimension. Usually the critical distance has to be chosen a bit smaller in order to avoid too many overlapping atom pairs. As well-suited distances R_{Cr} we found the following values:

	R_{NN}	R_{Cr}
1-d	$0.5\, n_{1D}^{-1}$	$0.26\, n_{1D}^{-1}$
2-d	$0.5\, n_{2D}^{-\frac{1}{2}}$	$0.15\, n_{2D}^{-\frac{1}{2}}$
3-d	$0.554\, n_{3D}^{-\frac{1}{3}}$	$0.5\, n_{3D}^{-\frac{1}{3}}$

It is also of interest how Rydberg atoms behave if they are located on a lattice structure such as in [Vit11]. In this case we cannot avoid overlapping pairs with the Hybrid model

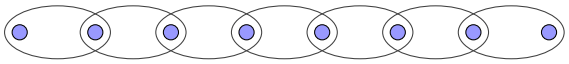

Figure 5.5: Usage of pairs in a lattice geometry in the Hybrid model.

and have to use a configuration like in figure 5.5. The problem of overlapping pairs is a systematic error in case of the lattice. However, such a model may still give qualitative predictions including the correlation effects.

In principle, it would also be possible to include even higher multiplets than pairs to improve the model's accuracy. In practice one would have to deal with even more overlapping pairs which is disadvantageous in general. Moreover, the computational effort to obtain the three-body steady state is very high: In the pair case one has to find the steady state of $(m^2)^2$ variables, where m is the number of states per atom, while for a triplet this would increase to $(m^2)^3$.

5.2 Technical Details

Just like for the rate equation (sec. 4.1.1), it is important to know when a single Monte Carlo run is to be stopped. Again we find that approximately $10 \cdot N$ Monte Carlo steps are sufficient to ensure convergency.

In order to know which atom number N the model is capable of, it is important to estimate the simulation's CPU time scaling behaviour as a function of N. We do not pay attention to the memory requirements here, since this is not critical.

Initialization: In the beginning atom positions have to be chosen. This is an independent procedure for each atom and thus scales with $\mathcal{O}(N)$. For special geometric realizations like a 1-d lattice the routine can be done in $\mathcal{O}(1)$.

Calculation of interaction potentials: It is time consuming to calculate the potential C_6/R^6 in every step. So usually it is a good idea to calculate all potentials in advance and store them for later use. As one can see from equation 2.5, all pairs have to be considered which makes this procedure scale with $\mathcal{O}(N^2)$. The problem to decide if two atoms should be treated as a pair can be done here, too.

Monte Carlo method: The Monte Carlo method is needed to bring the atomic configuration into the steady state. As mentioned before, the steady state is reached after $\approx 10 \cdot N$ Monte Carlo steps. Thus, this problem scales only with $\mathcal{O}(N)$. Note, however, that this procedure usually dominates the total runtime, since in every step a lot of non-trivial computations are needed, as described in section 4.1.2. We also note here that the calculation of a pair's steady state scales with m^{12}, where m is the number of states per atom. This highlights the importance of the few level approximation with $m = 2$ or $m = 3$. Actually, there is also a small component, which scales with $\mathcal{O}(N^2)$ here: During each step the effective potentials need to be updated. Still, the linear scaling of the steady state computations dominates the runtime.

Evaluation: For most of the observables the evaluation scales approximately with $\mathcal{O}(N)$. As seen in section 4.1.3, we need to calculate each atom's steady state for a fast

evaluation. In contrast to the rate equation model, we also have to consider the steady state of the pairs here, which makes the fast evaluation method a bit different: It might happen that an atom is part of different pairs (overlapping pairs). In this case we have to average all the pairs' contribution to this atom. If $g^{(2)}$-type observables are calculated in addition, the CPU time increases to $\mathcal{O}(N^2)$.

We record that the worst case scaling of the simulation is $\mathcal{O}(N^2)$, while for most purposes the critical part are the steady state computations during the Monte Carlo steps, which only scale linearly.

6 Performance & Limitations

In this chapter we want to discuss the capabilities of the models from a technical point of view. We can estimate the range of validity based on the approximations in these models and other general considerations. Moreover, we analyse the scaling of the runtime for the different models.

6.1 Range of Validity

We start our analysis with the mean-field model (sec. 2.3.1). Its fundamental approximation is $\rho^{(i,j)} = \rho^{(i)} \cdot \rho^{(j)}$, that means, the atoms are uncorrelated. In cases where these correlations are of importance, the model will break down. It also means, that the model is not capable of calculating $g^{(2)}$-type observables such as the pair correlation function (sec. 7.3) or the Mandel Q parameter (sec. 7.4). However, it is very easy to implement, one has access to the system's state at any time and to all the atoms' coherences. Regardless, it cannot reproduce the collective oscillation effect shown in sec. 1.2.2. If we have N interacting particles as considered in this work, the model also contains spatial information about excitation probabilities, just as all the other models which are discussed here. If the mean-field model is used as a one-particle method with a mean potential V_{Mean} (see sec. 2.3.1) then one does not have this information. Since the mean-field model is very fast in general one can simulate around 10^4 atoms with ease.

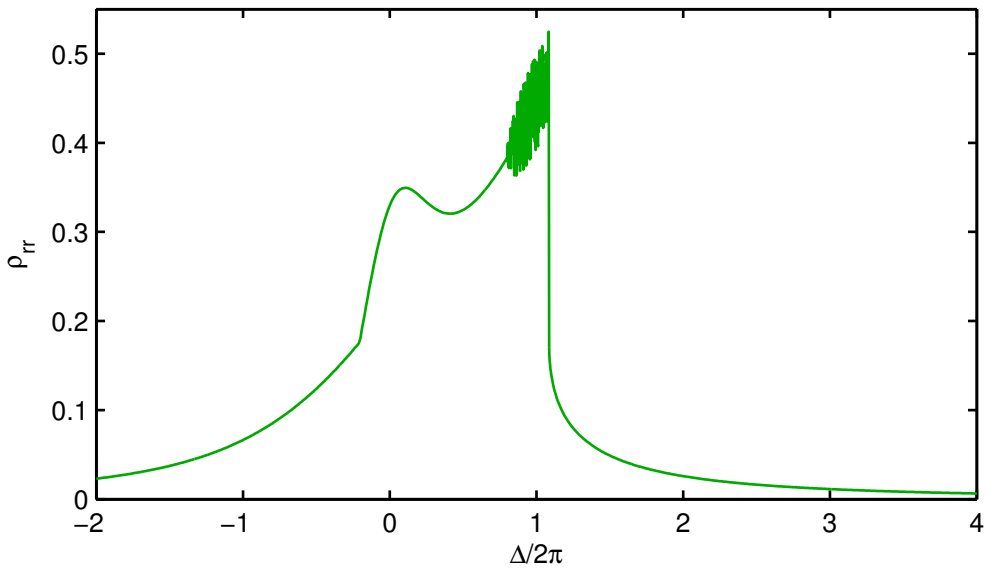

Figure 6.1: Problem with the mean-field model at low particle numbers: Non-physical drop-offs and oscillations occur. Parameters: $N = 2, \Omega_{12} = 2{\cdot}2\pi, \Omega_{23} = 1{\cdot}2\pi$, $\gamma_{21} = 6 \cdot 2\pi, \gamma_{32} = 1/40 \cdot 2\pi, \Gamma_{32} = \Gamma_{21} = 0.1 \cdot 2\pi, V = 2.5 \cdot 2\pi$.

The mean-field model with only a few atoms as well as the mean-field model which uses only effective single particle equations and a mean potential V_{Mean} are not applicable in some cases. If observables are plotted in dependence of the laser detuning, some non-physical phenomena can occur. In figure 6.1 we plotted $\rho_{rr}(\Delta)$. We included only two atoms in the simulation and an interaction potential of $V = 2.5 \cdot 2\pi$. It can be seen that the approximately expected Lorentzian profile is covered by an additional structure. The strong oscillation and the sharp drop-off in the resulting curve do not vanish even for long times and probably indicate that the system of differential equations is ill-conditioned. In any case, the mean-field model does not perform very well here. Also, one can expect that it will also fail in situations where atoms are located on a lattice structure, because then this effect would be occurring multiple times at the same position.

We conclude that the non-linear equations in the mean-field model give rise to some problematic characteristics. However, for a larger set of atoms in a random sample many different interaction strengths and positions exist, such that this non-physical behaviour is smeared out over a large range of detunings and in general not visible anymore.

The cluster expansion models (both the ladder approximation LA and the screened ladder approximation SLA) are designed to contain two-particle correlations. Thus, the models can show collective time behaviour to a certain degree. One also has access to the more complicated observables like the pair correlation function. As already described in section 2.3.2, the LA only allows one interaction strength to be large for a given triple of atoms. A large interaction strength could be defined as any interaction between atoms, whose distance is smaller than the blockade radius (see sec. 1.2.2). Indeed, one can say that the LA is only suited if not more than two atoms are inside a blockade volume at the same time. This also means that the LA should not be used for a lattice geometry, because then two interaction potentials out of a set of three neighbouring atoms are of the same strength. The cluster expansion with SLA, though, includes all interaction terms and thus should give consistent results beyond this limit. Note that for higher densities higher order correlations might become important, such that the model will also break down at some point. As we will see in section 6.2, the cluster expansion with LA is acceptably fast for atom numbers in the order of several 100 up to 1000 atoms.

The cluster expansion technique has a big disadvantage, though. It is designed to conserve the trace of the density matrix and thus the probability (see eq. 2.21), but not the purity of the system. The purity is defined as $\mathrm{Tr}(\rho^2)$ [Sch04]. The purity is one if the system is in a pure state: $\rho = \rho^2 = |\Psi\rangle\langle\Psi|$. If the system is in a mixed state, the purity is smaller than one. If we turn off the incoherent processes like spontaneous emission and dephasing, the system of N atoms evolves coherently and a pure state should always stay a pure state. In the following we calculate the time derivative of the purity:

$$\begin{aligned}\frac{d}{dt}\mathrm{Tr}(\rho^2) &= \frac{d}{dt}\left(\sum_l \sum_k \rho_{lk}\rho_{kl}\right) = \sum_l \sum_k \left(\dot{\rho}_{lk}\rho_{kl} + \rho_{lk}\dot{\rho}_{kl}\right) \\ &= 2\sum_l \sum_k \dot{\rho}_{lk}\rho_{kl} \end{aligned} \tag{6.1}$$

Using the coherent part of the master equation (eq. 2.9) only and applying it to $\dot{\rho}_{lk}$ immediately shows that the time derivative vanishes for the full N-atom density matrix $\rho^{(1,2,\ldots N)}$ as well as the mean-field expansion $\Pi_i^N \rho^{(i)}$. However, the expression does not vanish for the cluster expansion with LA and SLA in general. In some cases this turns out to be fatal. Especially if there is no damping (incoherent processes) in the system

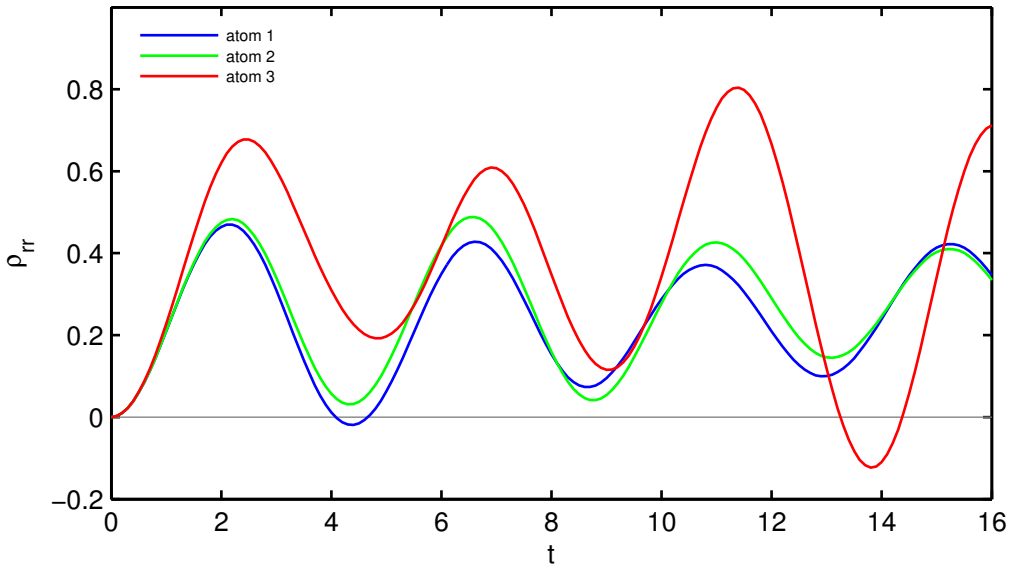

Figure 6.2: Breakdown of the cluster expansion I: negative population probabilities. Parameters: $N = 3, \Omega = 1, \gamma = \Gamma = \Delta = 0, V_{12} = 10, V_{13} = 1, V_{23} = 0.8$

the calculation might collapse. One situation is shown in figure 6.2. Here we used a two-level system, three atoms and the cluster expansion with LA. One can clearly see the non-physical effect in the simulation: the probabilities for atoms 1 and 3 become negative. This is due to the fact that the purity of the single atom's subsystem $\rho^{(i)}$ becomes larger than one. An exact three-body calculation would give purities in the range between one and zero. A purity larger than one, however, does not represent a physical density matrix anymore. The density matrix is still Hermitian and its trace is one, but is not longer positive semi-definite. The purity itself can be seen in the case of the cluster expansion with SLA. The formula from equation 2.21 can be used to construct the three-atom density matrix. Its trace and purity is plotted in figure 6.3. For $t = 0$ the purity is one, because the initial condition for the system is that all atoms are in the ground state, which means that we start with a pure state. For larger t the damping causes the system to evolve into a mixed state and the purity becomes less than one. At high t the purity becomes larger than one, which means the system is not in a physical state anymore.

The cluster expansion with SLA showed these problems very often during our simulations. Only with damping terms and $\Delta_{23} \leq 0$ (which is the more uninteresting part of the detuning as we will see in section 7.3) the simulation performed well. For the cluster expansion with LA, the non-physical behaviour only occurred if the damping terms were set to zero. In an experiment one always has to deal with incoherent processes, so the limitation for the cluster expansion with LA is not too problematic. The SLA, however, does not work with damping in general.

Next we want to focus on the rate equation. As already seen in figure 5.1, the rate equation cannot describe two-photon effects which appear in the two-atom master equation or even higher order of correlations. Moreover, only steady states can be calculated which restrains the parameters and observables to time-independent ones. For example, settings in which laser chirps are of interest (such as in [PDL10]) cannot be modelled

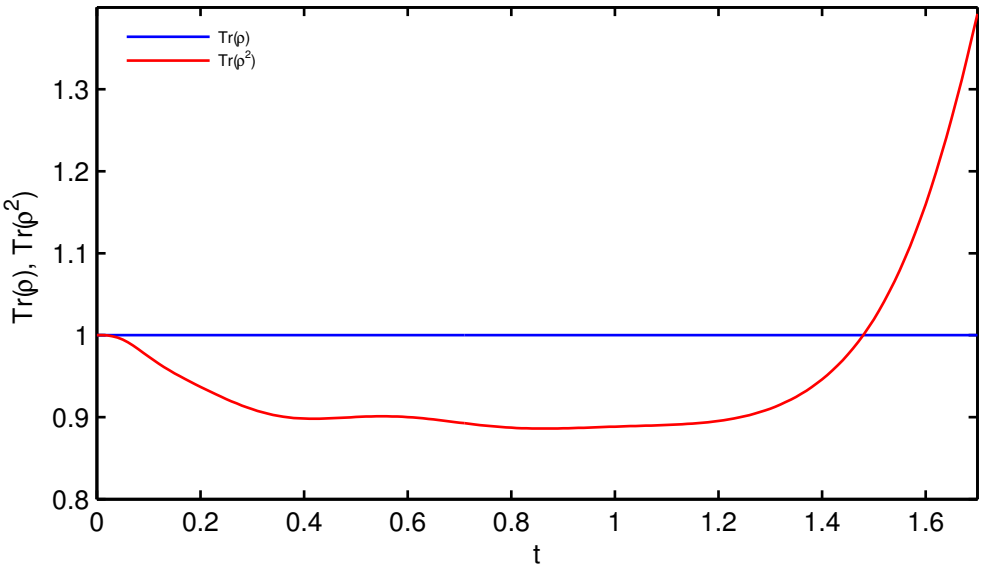

Figure 6.3: Breakdown of the cluster expansion II: The purity becomes larger than one, which indicates a non-physical state. Parameters: $N = 3, \Omega_{12} = 2 \cdot 2\pi$, $\Omega_{23} = 1 \cdot 2\pi, \Delta_{23} = 2.1 \cdot 2\pi, \gamma_{21} = 6 \cdot 2\pi, \gamma_{32} = 1/40 \cdot 2\pi, \Gamma_{32} = \Gamma_{21} = 0.1 \cdot 2\pi$, $V_{12} = 2.78, V_{13} = 433.69, V_{23} = 2.04$

with rate equations. The incapability of calculating a dynamic solution is originally caused by negative coefficients (see sec. 2.3.3). For a given set of parameters it is usually possible to find a new basis, such that the rate equation obtained from the equations of motion in this basis has only positive coefficients. The only variable which is usually changed during a single Monte Carlo run is the laser detuning, because it also absorbs the interaction energy, which might change after every jump. Therefore, it is necessary to find a set of bases (each with an interval where all rates are positive) which cover all values $\Delta \in \mathbb{R}$. Unfortunately, the transformation between the bases demands the knowledge of the exact coherences, which have been eliminated in the first place. Thus, this ansatz does not work. Currently, we see no possibility to obtain the time evolution for a rate equation in general. A completely positive attribute is the high number of atoms which the model is capable of, though. It is absolutely no problem to do simulations with several 1000 atoms.

In the end we want to look at the Hybrid model. Just as the rate equation it cannot be employed for time-resolving simulations, but only predicts the steady state of a system. The model includes second order correlations for atoms whenever they are part of a pair in the configuration. The accuracy is decreased if these pairs overlap (sec. 5.1.1). Usually one has to work with a maximum distance up to which atoms are treated as a pair (sec. 5.1.2). This also means, that beyond this distance the two particle correlations are not taken into account exactly anymore. If one wants to compute the pair correlation function (sec. 7.3), for instance, it will only include exact pair effects to this critical distance, even though they might also be important for larger separations. The model is capable of quite large numbers of atoms: up to some 1000 atoms can be simulated in an acceptable time.

6.2 Runtime

A very important quantity to characterize the models are their runtime. In general the time should be as low as possible. Our discussed models can be divided into two classes: First, we have the rate equation and the Hybrid model which are plain Monte Carlo simulations. This means, for every setting the simulations have to be carried out numerous times. As pointed out in section 4.1.3 the calculation of $g^{(1)}$-type observables can be improved a lot, but for more complicated observables, such as the pair correlation function, this speedup does not work and an individual atom count has to be done. Especially at large detuning, where Rydberg excitation becomes less probable, the number of simulations and thus the runtime increases a lot. The second category consists of the mean-field model and the cluster expansion. One single simulation already gives good results for every observable, since the exact probabilities are known. Nevertheless, many realizations need to be carried out and averaged to compensate the fact that we have fewer atoms in the simulation than in an experiment. In special cases, such as in a lattice geometry, a single simulation is sufficient. We also note that the memory requirements are a negligible quantity compared to the CPU time. In the following all simulation times were measured on a single 3.40 GHz core.

The rate equation and the Hybrid model are only capable of calculating the steady state, therefore the runtime for a single simulation is easy to define. The other models, though, can calculate the dynamics in addition. The runtime strongly depends on the parameter choices as well as the time which shall be simulated. This is why we need a standardised setting to quantify the runtime.

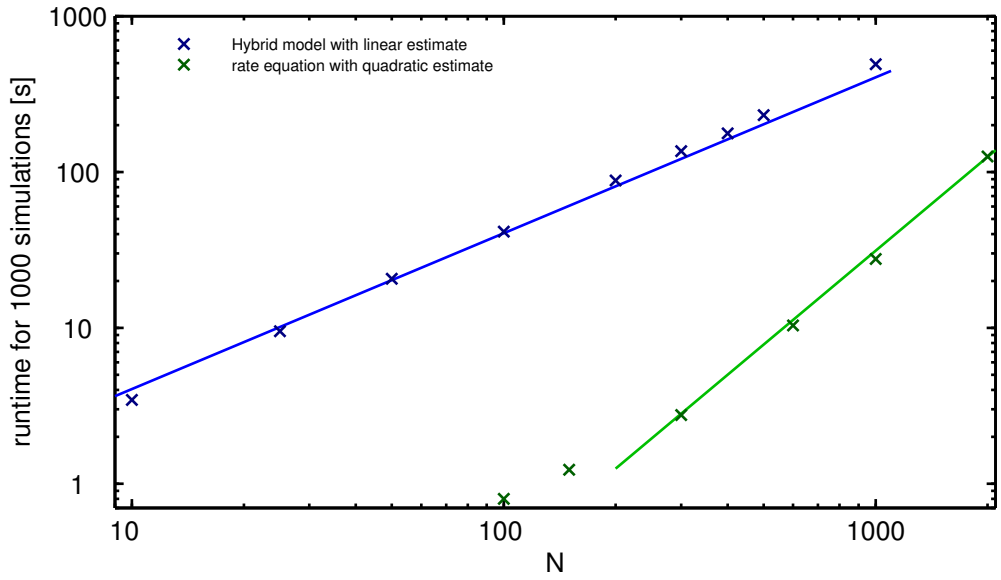

Figure 6.4: Runtime of the Hybrid model and the rate equation with our implementation for a typical set of parameters.

The runtime of 1000 simulations for a different number of atoms N of the rate equation and the Hybrid model with our implementation is plotted in fig. 6.4. Of course, the rate equation performs better because only single atom steady states and not pair steady states have to be calculated. As pointed out in section 5.2 the numerical effort of the hybrid model scales with $\mathcal{O}(N^2)$ in general, but because of the time consuming process

of the steady state calculation the main contribution to the runtime is only linear in N. This can be seen for the Hybrid model: Over a big range the linear fit agrees with the data points quite well. In general the slope is steeper which indicates that the $\mathcal{O}(N^2)$-contribution is present. In the case of the rate equation the numerical effort for the calculation of the steady states is much lower and thus the quadratic behaviour appears clearly. Only for low atom numbers the scaling approaches a linear dependence.

For analysing the runtime of the cluster expansion and the mean-field model we choose the parameters from [Sch10] and a density of $n_{3D} = 1.3 \cdot 10^{-3}$. The maximal distance to which atoms are treated as correlated (see sec. 4.2) was set to $L_{Cr} = 15$. The resulting runtimes can be seen in fig. 6.5. Each data point was averaged over several spatial

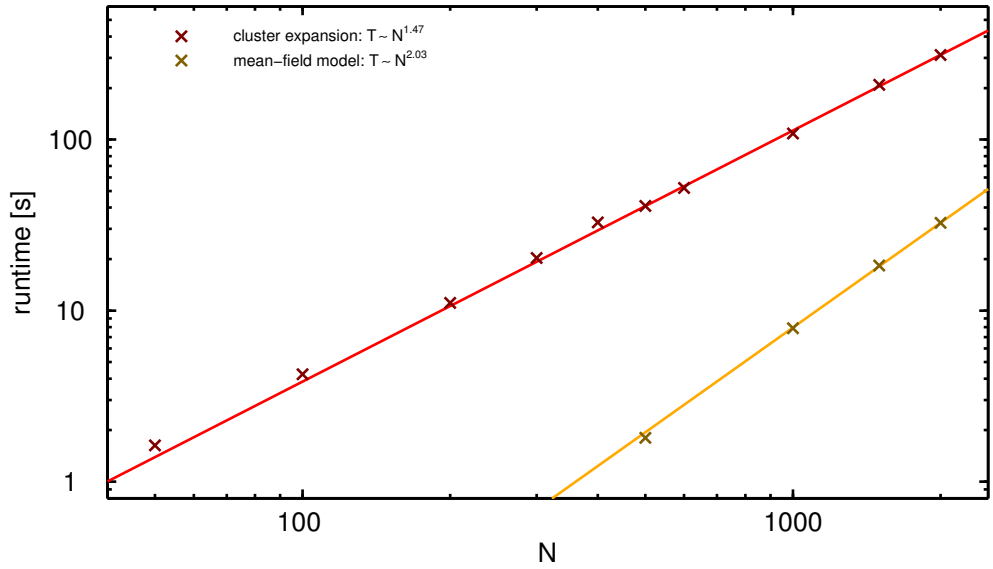

Figure 6.5: Runtime of the cluster expansion and the mean-field model with our implementation for the standardised set of parameters described in the text.

realizations as well as over different values for the laser detuning. The mean-field model performs very well and shows a quadratic dependence on N. This is due to the fact that the mean-field model and the cluster expansion use the same code base in our case. As mentioned in section 4.2 the table $\sum_{k\neq i} V_{ik}\rho^{(i,k)}_{\cdot\cdot,rr}$ for every atom i is constructed. This is a $\mathcal{O}(N^2)$ process. In case of the mean-field model this falls back to $\rho^{(i)}_{\cdot\cdot} \sum_{k\neq i} V_{ik}\rho^{(k)}_{rr}$, but still causes a quadratic runtime. Apparently, this dominates the total runtime for a large number of atoms. On the other hand, the cluster expansion shows a lower scaling. The creation of the table still needs a quadratic time but is not the dominating process here. As pointed out in section 4.2, the number of variables approximately scales linearly with the number of atoms. For a high number of variables other effects, such as the plain integration, are dominating over the $\mathcal{O}(N)$ process. Hence, the overall result is a scaling in between $\mathcal{O}(N)$ and $\mathcal{O}(N^2)$.

In absolute numbers the Monte Carlo methods are much faster than the dynamics resolving models. However, one needs to remember that it also depends on the observable and the parameters to decide which model can produce a faster and more accurate result.

7 Physical Capabilities & Results

In this chapter we want to apply the discussed models to realistic physical setups and calculate various observables. Our aim is to decide which model can describe the given physical situation the best. We also make some observations which have not been discussed in the literature yet.

We start with a rather simple observable: the Rydberg excitation probability. Then we take a closer look at a setting where EIT properties are analysed [ASP11]. After this we discuss the pair correlation in detail. Finally we look at the system's counting statistics of excitation numbers.

7.1 Excitation Probability

One of the most important observables is the Rydberg excitation probability. Early works as well as more recent articles focused on the Rydberg excitation, analysed the dependence on the cloud's density [Sin04; Ton04] and looked at the shape of the Rydberg resonance by varying the upper laser detuning Δ [Sch10]. As seen in section 1.2.2 the total number of excitations should saturate with increasing atom density. In fact, all models reproduce this feature, which can be seen in figure 7.1 for a representative set of parameters. The excitation probability decreases with increasing density (and thus larger interaction effects). Moreover, the resonance shifts to larger detunings. Especially the mean-field model has a pronounced shift and a large width for high densities. As reported in [Sch10] the mean-field model overestimates these effects and does not reproduce the experimental data. The broadening and the shift of the main peak can be understood if we remember the curve from figure 6.1, where the same curve was plotted for $N = 2$: There we obtain a sharp drop-off in the plot for $\Delta > 0$ which is caused by the strong simplifications in the model. Here, in the 3-d random sample, the drop-off is averaged out due to the nearly continuous distribution of interaction energies in the system, but still causes the main peak to be farther from $\Delta = 0$ and to be broadened. Thus, the predictions of the other three models should be more accurate. The Hybrid model does not give new results compared to the rate equation model, because exact two-particle interaction effects are not important for this observable. The cluster expansion shows a suppression of the maximum values of ρ_{rr} in the range of the other models, but has a much smaller shift of the main resonance peak. This can be understood by the fact that the model was designed for rather low densities where only a few atoms are inside one blockade volume (sec. 2.3.2). For the higher densities considered here, this condition is not fulfilled anymore. The effects of stronger interaction might be underestimated. In lower dimensional samples the same qualitative features are present.

In order to see a more pronounced difference between the models, we now look at another spatial configuration: a 1-d lattice geometry with lattice constant $a = 5.2$. As pointed out in section 5.1.2 and figure 5.5 the Hybrid model has to work with overlapping pairs and a systematic error has to be expected. But also the cluster expansion

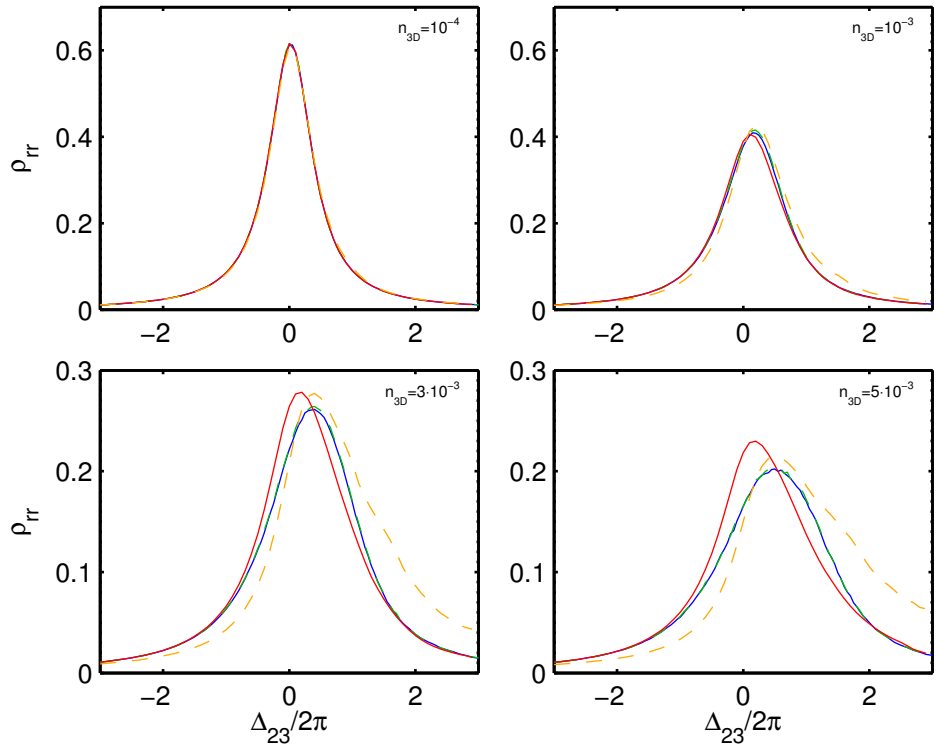

Figure 7.1: Steady state values of ρ_{rr}. Hybrid model (blue), rate equation (green), cluster expansion (red), mean-field (orange). Parameters: $\Omega_{12} = 2 \cdot 2\pi, \Omega_{23} = 1 \cdot 2\pi$, $\gamma_{21} = 6 \cdot 2\pi, \gamma_{32} = 1/40 \cdot 2\pi, \Gamma_{32} = \Gamma_{21} = 0.1 \cdot 2\pi, C_6 = 310000$.

reaches the limit of its validity here: If we consider three atoms, then two large and one small interaction strengths are present in the system, but the LA is only designed for one large interaction (see sec. 2.3.2). Also note that the cluster expansion and the mean-field model do not need Monte Carlo sampling on a lattice at all. Again we look at the steady state value of the Rydberg excitation probability. The result for the case with the same parameters as in figure 7.1 is depicted in figure 7.2. We first focus on the explanation of the rate equation's curve. The main peak is located at position $\Delta_{32} = 0$, which corresponds to the resonance in the non-interacting case. The interaction of two neighbouring atoms is $V = \frac{C_6}{a^6}$. If an atom is excited to a Rydberg state, a neighbouring atom thus sees an effective detuning of $\Delta_{\text{eff}} = \Delta_{23} - V$. In the case of figure 7.2 the potential is $V = \frac{C_6}{a^6} \approx 2.5 \cdot 2\pi$, thus the effective detuning vanishes for $\Delta_{23} \approx 2.5 \cdot 2\pi$ and the resulting resonance is clearly visible. The Hybrid model also covers these effects, but shows an additional structure in the middle of the two main resonances. This arises from the included 2-γ-transitions. Two neighbouring atoms can be excited at the same time and share the necessary detuning which is needed to overcome the interaction potential: The process $|mm\rangle \leftrightarrow |rr\rangle$ is resonant at $2\,\Delta_{23} = V = \frac{C_6}{a^6}$. The cluster expansion model also shows this resonance, but predicts a larger peak. This can be understood by recalling that the Hybrid model only takes into account this process half because of the overlapping pairs. In the range of $V \approx \Delta_{23}$ the cluster expansion model shows a sharp drop-off. This becomes more pronounced the more atoms are used in the simulation and vanishes if only a few atoms are considered. Possibly, it is a similar effect as in the mean-field calculations. As already expected in section 6.1, the mean-field model on a

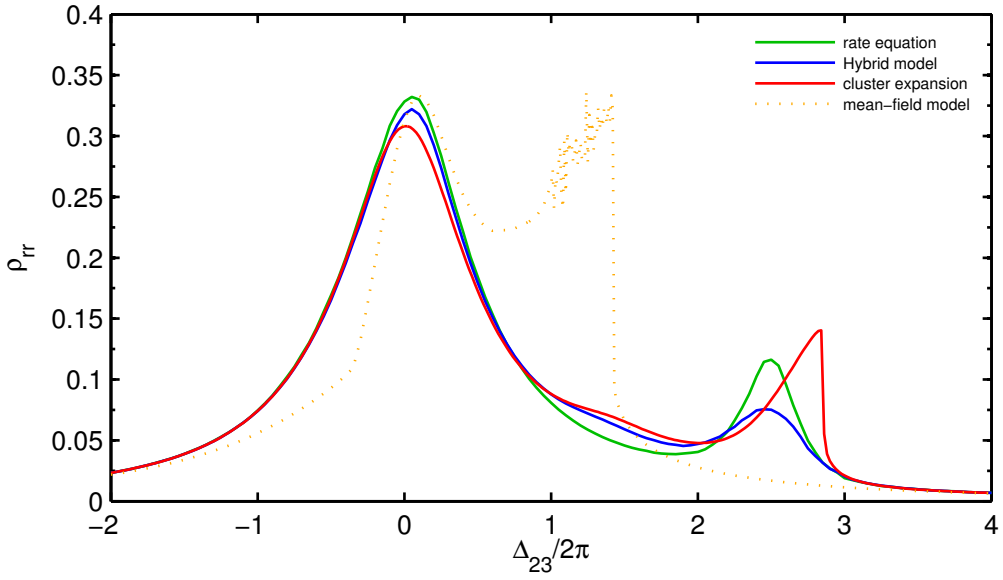

Figure 7.2: Rydberg excitation probability on a 1-d lattice.

lattice shows the same problems as in a two-particle calculation: The rapid oscillations, which do not vanish over time, are present just left of the drop-off.

We conclude that the mean-field model is not suited to describe the most fundamental observables on a lattice structure. The rate equation and the Hybrid model give more plausible results. In addition, the Hybrid model shows the two-photon resonance. The cluster expansion agrees with its predictions qualitatively, but seems to have a numerical limitation at $V \approx \Delta_{23}$. In a random sample we saw that the mean-field model gives unreasonably large shifts in the resonance peak and the cluster expansion reaches its limits. The Hybrid model shows exactly the same features as the rate equation here and seems to be a good candidate for predicting the excitation probability at moderate densities.

7.2 Laser Absorption and EIT

The three-level system of each atom can be used to perform an EIT experiment [FIM05]. Without interaction, each atom propagates into the EIT dark state $|D\rangle \approx \Omega_{23}|g\rangle - \Omega_{12}|r\rangle$. For $\Gamma_{31} = 0$ this dark state is approximately the atom's steady state, because γ_{32} is small compared to other parameters and thus the dark state hardly decays. This means all atoms behave as an EIT system and typical EIT features can be seen. Its main characteristic is that the laser absorption vanishes. For the coupling Ω_{12} the laser transmission T is described by the imaginary part of the susceptibility, χ_I. This quantity is related to the coherence of the corresponding transition: $\chi_I \sim \Im(\rho_{gm})$ [SZ97]. As pointed out in [ASP11], this is proportional to the intermediate state's population ρ_{mm} in the steady state:

$$-\log T \sim \chi_I \sim \Im(\rho_{ge}) \sim \rho_{mm} \tag{7.1}$$

With this relation we can calculate the laser transmission, which is an experimentally accessible quantity (see [Pri09; Pri10; Tau10]), with all our models. For low densities,

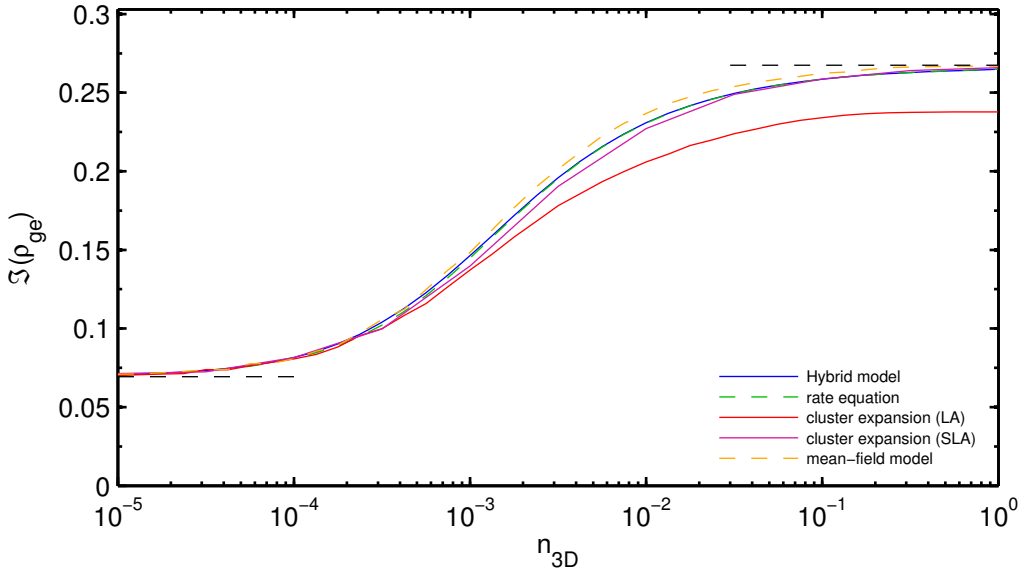

Figure 7.3: $\Im(\rho_{ge}) \sim -\log T$: the laser transmission strongly depends on the density. Black dashed lines: analytical low density and two-level limit. Parameters: $\Omega_{12} = 2 \cdot 2\pi$, $\Omega_{23} = 1 \cdot 2\pi, \gamma_{21} = 6 \cdot 2\pi, \gamma_{32} = 1/40 \cdot 2\pi, \Gamma_{32} = \Gamma_{21} = 0.1 \cdot 2\pi$, $\Delta_{12} = \Delta_{23} = 0, C_6 = 310000$.

and thus hardly any interaction between the atoms, the transmission is close to one. The deviation is because of the instability of state $|r\rangle$ and of the coherence ρ_{gr} due to spontaneous emission and dephasing. Beside this, the system behaves like in an ideal EIT case. For higher densities the interaction blocks the population of Rydberg states and hence the dark states, too. In general the state $|m\rangle$ is populated to a rather high degree and the laser transmission decreases. As measured in [Pri09; Pri10], this happens in a non-linear way when one varies the density or the laser strength Ω_{12}. These effects could be modelled successfully in [ASP11] by using the rate equation model. In figure 7.3 the non-linear behaviour of the laser transmission is shown as a function of the density. For low densities we can estimate the value for $\Im(\rho_{ge})$ by calculating the steady state value of a single non-interacting atom. For the high density limit the system contains only a few Rydberg excitations and for most other atoms the Rydberg level is blockaded. Consequently, most atoms behave as a two level system of states $|g\rangle$ and $|m\rangle$ [ASP11]. Both these limits are plotted in figure 7.3 as dashed black lines. For all models, except the cluster expansion, these values are reached. The deviation of the cluster expansion model can be explained by the fact that it is not designed for high densities, just as reported in [ASP11]. However, if we do not use the LA but the SLA approximation (see sec. 2.3.2) the simulation shows the right high density limit. Note that the SLA does not work in general, our parameters are in the range of the model's applicability (see sec. 6.1). Interestingly, the mean-field model covers the more complicated models' data pretty well, but overestimates the values a bit. This can be understood by noting that we are at zero detuning, where the value for ρ_{rr} is generally lower than for other models (see fig. 7.1). Therefore, the population probability of ρ_{mm} and thus the coherence value $\Im(\rho_{ge})$ is higher. The Hybrid model yields the same results as the rate equation. This is not surprising for two reasons: First, the Hybrid model is based on the rate equation. Secondly, the use of pairs in the Hybrid model is limited up to a certain atomic distance

(see sec. 5.1.2). For the rather high densities which are considered here, this critical distance is way smaller than the blockade radius and the benefits from the Hybrid model, such as two-photon resonances, do not occur at all.

In conclusion we note that the qualitative behaviour of all models is basically the same with the exception of the cluster expansion model, which is not suited for high densities. The Hybrid model gives consistent results, but the use is unnecessary in the considered case, because it falls back to the rate equation model.

We remark that also different methods such as approaches with non-Hermitian Hamiltonians [Res11], a quantized radiation field [POF11] and analytic expansions in Ω_{12} [Sev11a] were used to explain some EIT features in Rydberg systems.

7.3 Pair Correlation

We have already seen in section 1.2.2 that the interaction does not allow nearby atoms to be excited at the same time. To quantify this, we introduce the blockade radius R_B (cf. [CP10]). A pair is blockaded if the interaction energy exceeds the width of the resonance of $|rr\rangle$ with respect to Δ_{23}. A simple estimation for the blockade radius at zero detuning at low densities is found in [CP10]:

$$R_B \approx \left(\frac{C_6}{\Omega_{23}}\right)^{\frac{1}{6}} \tag{7.2}$$

With our models we are able to compute a quantity which describes the correlation of a pair with a certain interatomic distance – the pair correlation function $g^{(2)}(r)$. In [Wüs10] it is defined as:

$$g^{(2)}(r) = \frac{1}{\sum_{i,j}{}^{(r)}\, 1} \cdot \sum_{i,j}^{(r)} \frac{\langle S_{rr}^{(i)} S_{rr}^{(j)} \rangle}{\langle S_{rr}^{(i)} \rangle \langle S_{rr}^{(j)} \rangle} \tag{7.3}$$

Here $\sum_{i,j}{}^{(r)}$ denotes the sum over all pairs with distance r:

$$\sum_{i,j}^{(r)} = \sum_{\substack{i,j \\ |R_i - R_j| \in [r, r+dr)}} \tag{7.4}$$

Working with this definition, however, is not possible for the rate equation and the Hybrid model, since we do not know the occurring fraction with the expectation values for a given pair. We can only calculate each expectation value separately by averaging over many realizations. Therefore we use the definition which can be found in [HR06]:

$$g^{(2)}(r) = \frac{\sum_{i,j}{}^{(r)} \langle S_{rr}^{(i)} S_{rr}^{(j)} \rangle}{\left(\frac{1}{N} \sum_i \langle S_{rr}^{(i)} \rangle\right)^2 \cdot \sum_{i,j}{}^{(r)}\, 1} = \frac{\sum_{i,j}{}^{(r)} \langle S_{rr}^{(i)} S_{rr}^{(j)} \rangle}{\rho_{rr}^2 \cdot \sum_{i,j}{}^{(r)}\, 1} \tag{7.5}$$

This quantity can be calculated with the rate equation and the Hybrid model. Note that it is a $g^{(2)}$-type observable and thus needs more statistics to obtain smooth values (sec. 4.1.3). The definitions 7.3 and 7.5 give the same values, if $\langle S_{rr}^{(i)} \rangle = \langle S_{rr} \rangle = \rho_{rr}$, that means the excitation probability is independent of the atom's position. This holds if we have a homogeneous density and can neglect boundary effects of the trap. In the

calculations we used a 1-d trap and a large number of atoms, such that the ends of the trap do not influence the observables too much. The pair correlation function can also be calculated with the cluster expansion model. Here both the definitions 7.3 and 7.5 can be used. From mean-field calculations, though, this quantity cannot be obtained, because its basic assumption is "no correlation" ($\rho^{(i,j)} = \rho^{(i)} \cdot \rho^{(j)}$) which would only make the fraction in the definitions equal to one.

The pair correlation function gives one if the atoms are independent of each other (in terms of Rydberg excitations) and gives zero if they cannot be excited to a Rydberg state at the same time, that means the Rydberg blockade acts on the pair. At $g^{(2)}(r) > 1$ the double excitation probability is enhanced compared to the independent case.

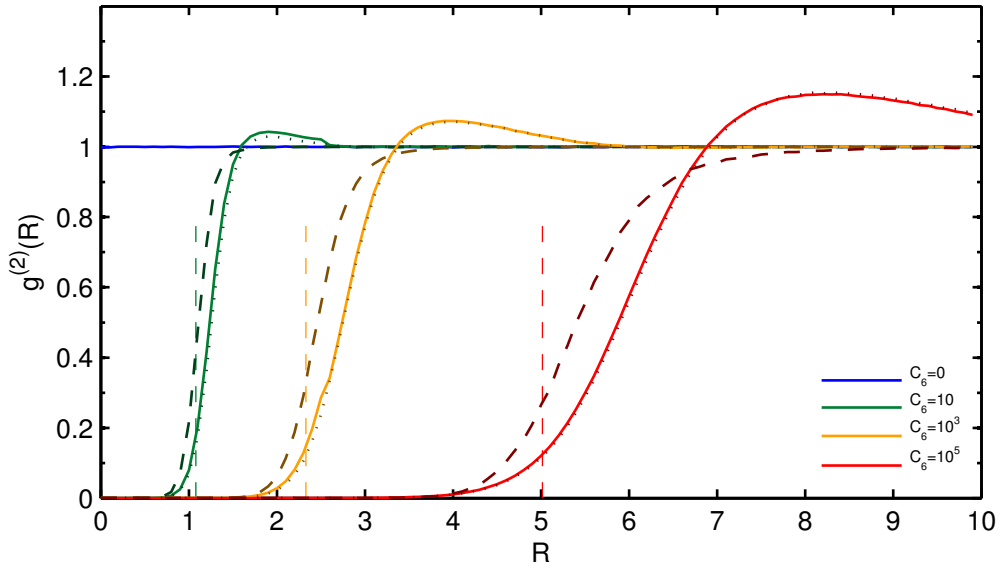

Figure 7.4: Pair correlation $g^{(2)}$ for different C_6: Hybrid model (solid), rate equation (dotted), cluster expansion (dashed). Blockade radius estimation from eq. 7.2 are shown as vertical lines. Parameters: $\Omega_{12} = 2 \cdot 2\pi, \Omega_{23} = 1 \cdot 2\pi, \gamma_{21} = 6 \cdot 2\pi$, $\gamma_{32} = 1/40 \cdot 2\pi, \Gamma_{32} = \Gamma_{21} = 0.1 \cdot 2\pi, \Delta_{12} = \Delta_{23} = 0$.

In figure 7.4 the $g^{(2)}(r)$ function is plotted for the Hybrid model, the rate equation and the cluster expansion, using different C_6. In the case of no interaction, that means $C_6 = 0$, the pair correlation is in fact always one, as expected. At non-zero interaction strength, the blockade becomes visible: From $r = 0$ up to some value depending on C_6, the pair correlation function is zero. In the case of the Hybrid model and the rate equation, the $g^{(2)}$ function becomes even bigger than one for larger r, which can be interpreted as a formation of a crystal structure: In the non-interacting system the probability of a Rydberg excitation is approximately $\Omega_{12}^2/(\Omega_{12}^2 + \Omega_{23}^2) = 0.8$, so due to the laser parameters many excitations are preferred. In order to maximize the number of excitations, the system automatically evolves into a dense packing of Rydberg atoms. The pair correlation function shows only one maximum, in contrast to a real periodic crystal. Thus, it is intuitive to think of a fluid of Rydberg excitations if we are looking at our system in the steady state. Interestingly, the cluster expansion model does not show this behaviour at all. It remains an open question which model describes the true physics. This exact shape of the $g^{(2)}$ function is, for example, important when the mean-field potential in mean-field models has to be calculated (see [Wei08]). Especially

the values at small distances have a big influence. We note that the shape of the pair correlation function strongly depends on the chosen parameters: A larger density, a larger laser coupling or smaller decay rates seem to cause more and stronger oscillations for large distances. However, we do not focus on these effects in the scope of this work.

We also see that a larger C_6 coefficient causes a bigger blockade radius. This radius agrees with the estimated value in equation 7.2. For large distances the interaction has no impact anymore and the pair $g^{(2)}$ function becomes one, as in the case of non-interacting atoms.

We want to put our focus on the difference of the Hybrid model and the rate equation now. For our chosen set of parameters the curves are pretty similar in general, but show small deviations for small distances: For $C_6 = 10$ and $C_6 = 10^3$ the Hybrid model gives slightly higher values than the rate equation. At $r > 2.6$ the two curves coincide again, because this is just the critical distance up to which two atoms are treated as a pair (cf. sec. 5.1.2).

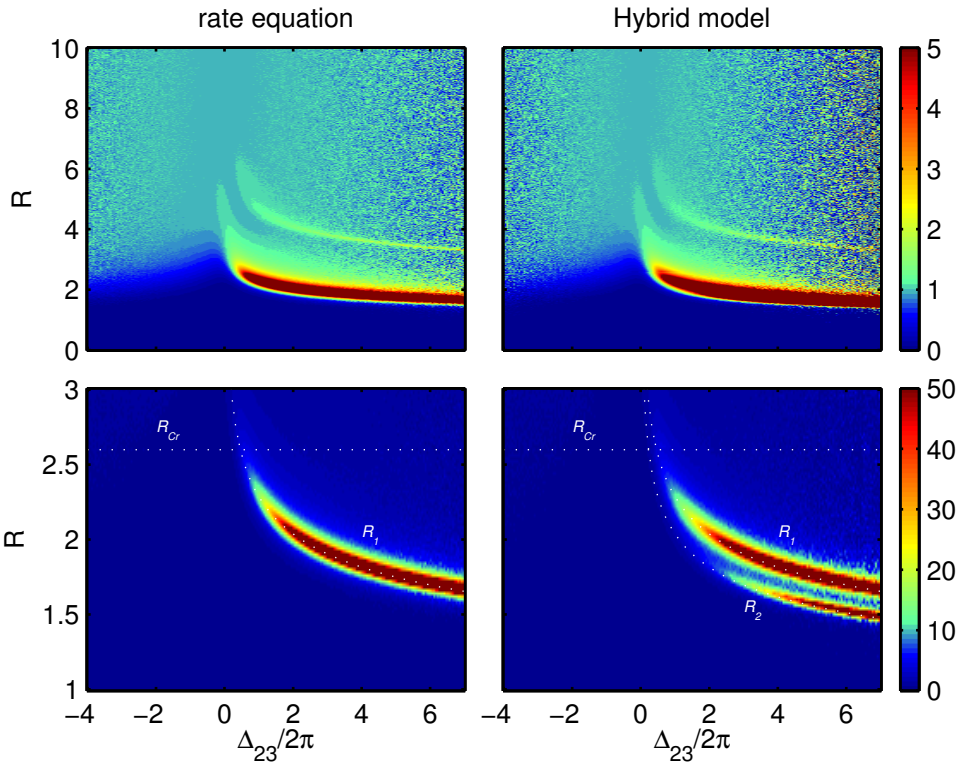

Figure 7.5: $g^{(2)}(r, \Delta_{23})$ with rate equation and Hybrid model.

While figure 7.4 was calculated with zero laser detuning, it is also of interest how the pair correlation function behaves for non-vanishing values of Δ_{23}. The result for the rate equation and the Hybrid model are illustrated in figure 7.5. The same parameters like in figure 7.4 and an interaction strength of $C_6 = 900$ were used. For all detunings the blockade region is clearly visible, as well as the uncorrelated regime for large distances. However, for intermediate distances resonances occur. This is the case if the detuning and the interaction cancel each other. In the case of the rate equation model we can easily identify the exact condition of the resonance. In the lower picture, which has a larger scale, the line $C_6/R^6 = \Delta_{23}$ was drawn. It fits the plot's maximum perfectly. We can interpret the resonance as follows: Assume an atom is excited to the Rydberg state.

Then, since the interaction partly acts as a detuning, a second atom sees the effective detuning $\Delta_{\text{eff}} = \Delta_{23} - V(R)$. If this effective detuning is zero, the excitation probability of the second atom is strongly enhanced, because the interaction as well as the detuning do not suppress this process any more. The corresponding distance is:

$$R_1 = \left(\frac{C_6}{\Delta_{23}}\right)^{\frac{1}{6}} \tag{7.6}$$

The argument can be expanded to a third atom: If its distance to the second atom is also R_1, then the excitation probability is also enhanced. In a 1-d geometry the distance between the first and third atom is then $2R_1$. This resonance, $R = 2\,(\frac{C_6}{\Delta_{23}})^{\frac{1}{6}}$, can also be seen in figure 7.5.

The Hybrid model shows the same basic features, but if we change the scale we notice that a new resonance line becomes visible. Its origin arises from the included 2-γ-effects. As discussed in sections 5 and 7.1, this process is resonant if $V = 2\,\Delta_{23}$. The condition for the distance is:

$$R_2 = \left(\frac{C_6}{2 \cdot \Delta_{23}}\right)^{\frac{1}{6}} \approx 0.89 \cdot R_1 \tag{7.7}$$

The corresponding line is also shown in figure 7.5 and matches the resonance's maximum perfectly. Moreover, the transition line of the Hybrid model R_{Cr} is plotted. One can see that the new resonance line occurs in the pair regime of the Hybrid model.

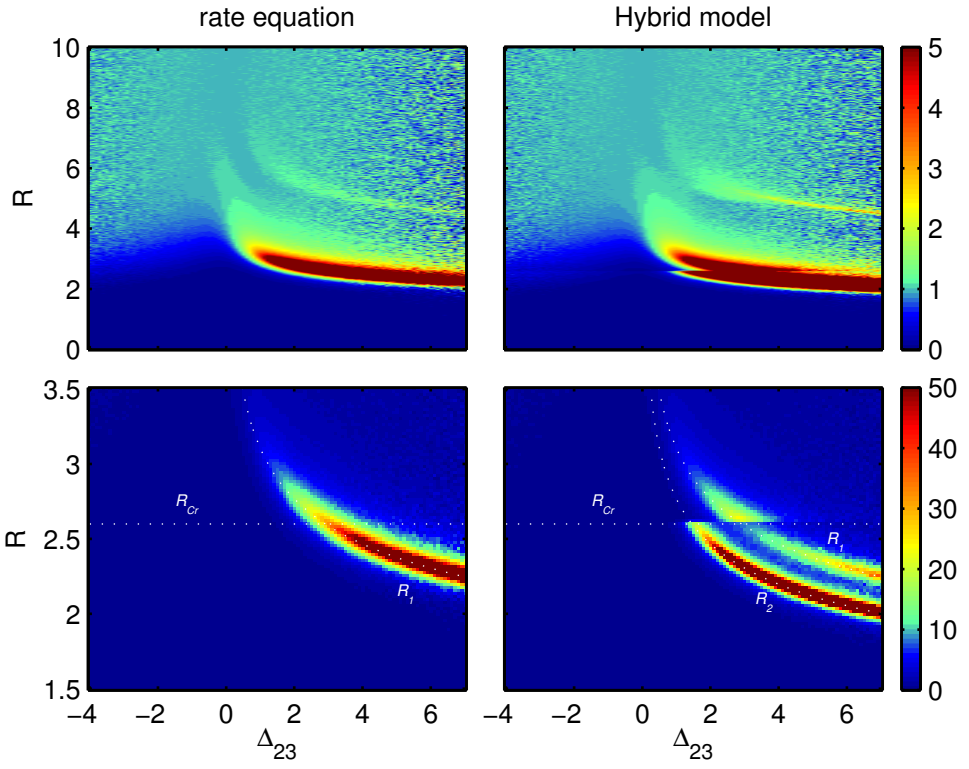

Figure 7.6: $g^{(2)}(r, \Delta)$ with rate equation and Hybrid model for a 2-level system. Parameters: $\Omega = 1, \gamma = 0.001, C_6 = 900, N = 500, n_{1\text{D}} = 0.1$. At $R_{Cr} = 2.6$ the Hybrid model falls back to the rate equation.

To confirm the resonance lines and our interpretation we performed a similar simulation for a two-level system (fig. 7.6). Compared to three states, we find a similar pattern. The main difference to note is the discontinuity in the Hybrid model's plots. At a distance of $R > 2.6$ the Hybrid model's pairs fall back into the steady state model's single atom treatment. We can clearly see that the 2-γ-process is solely a feature of the Hybrid model.

If we look at large detunings the results become very noisy. This is due to the fact that only very few Rydberg excitations are in the system and therefore it needs a lot of simulations and time to obtain good statistics.

So far we only discussed the properties of the plots which were created with the Hybrid model or the rate equation. Since the results in the zero detuning case are very different compared to the cluster expansion (fig. 7.4), it is of interest how the cluster expansion behaves for a non-vanishing laser detuning. We use the same parameters as in the 3-level

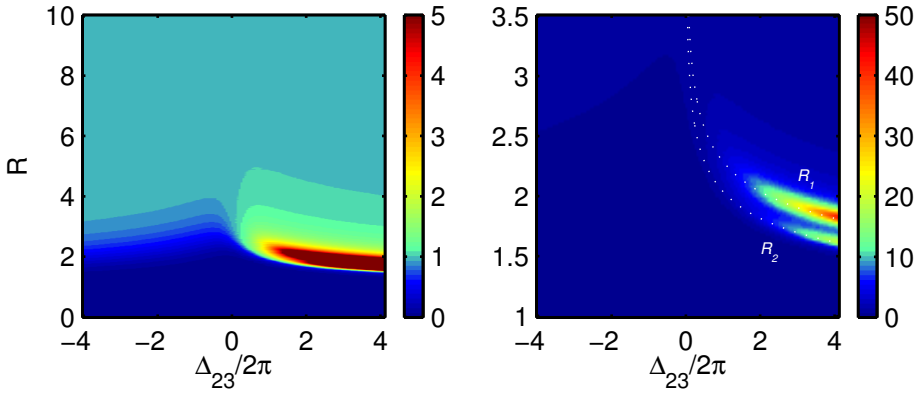

Figure 7.7: $g^{(2)}(r, \Delta_{23})$ with the cluster expansion model.

case of figure 7.5. The result of the cluster expansion simulation is depicted in figure 7.7. Just as in the discussed case, the same resonance lines 7.6 and 7.7 occur. This confirms our interpretation of resonant excitation processes. However, the actual value for $g^{(2)}$ at these values differ. The second big difference is the "third atom excitation line" at $2 \cdot R_1$. In figures 7.5 and 7.6 this line could be seen, because the models do also include the excitation of three atoms at the same time and thus three-body correlations, even though they might be incomplete. On the other hand, the cluster expansion only contains correlations of second order and cannot give any probability that three atoms with these distances are excited in the same time. Consequently, the line at $2 \cdot R_1$ does not emerge. Another notable difference between the models is the smoothness of the plotted figures. In the case of the Hybrid model as well as the rate equation the calculation requires two atoms with a certain distance to be in the state $|r\rangle$ at the end of a single simulation. For a large detuning this becomes unlikely and many Monte Carlo runs have to be performed to obtain usable statistics. In the case of the cluster expansion, however, we have direct access to the probabilities $\rho^{(i,j)}_{rr,rr}$ and so we need fewer statistics to achieve a good resolution.

In higher dimension the qualitative effects such as the resonance lines R_1 and R_2 stay present. Only the "three-body resonance" at twice the distance R_1 vanishes, since the distance between the first and third atom is not necessarily twice the distance between

atom one and two, and thus the resonance line is smeared over a large range of distances.

So far the simulations were performed with low dephasing rates. It is important to look at the effects of larger dephasing, since it occurs in any experiment. It turns out that the crucial rate is Γ_{31}, while the other rates do not have such a big influence on the simulation's results. The effect of the dephasing rate Γ_{31} is plotted in figure 7.8 with

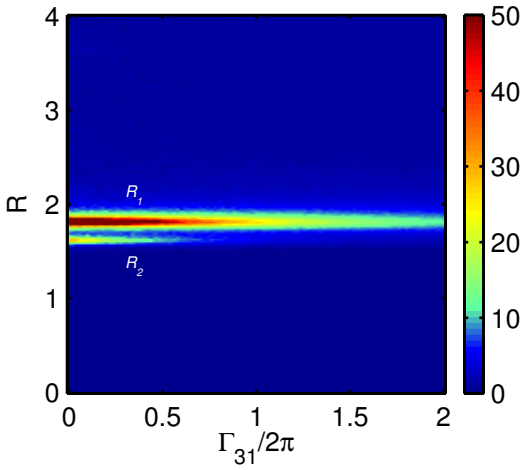

Figure 7.8: Pair correlation $g^{(2)}(r)$ for different dephasing Γ_{31} at $\Delta_{23} = 4 \cdot 2\pi$ with the Hybrid model.

the Hybrid model. The same parameters as in figure 7.5 and a detuning of $\Delta_{23} = 4 \cdot 2\pi$ were used. As one can see, the dephasing rate Γ_{31} should be small in order to see the double resonance structure. Somewhere between $\Gamma_{31}/2\pi = 0.5$ and 1 the 2-γ-resonance R_2 (eq. 7.7) vanishes in the background. The resonance R_1 (eq. 7.6) stays visible even for large dephasing rates, though.

We conclude that the Rydberg blockade can be seen in the pair correlation function. Defining a sharp blockade radius does not work in our setting, though. The transition from a fully blockaded to an uncorrelated regime is smeared out. If we look at non-zero laser detuning the $g^{(2)}$-function exhibits several maxima. These lines can be understood as resonant excitation channels where the laser detuning and the interaction energy cancel each other. The Hybrid model as well as the cluster expansion also show the $|mm\rangle \leftrightarrow |rr\rangle$ process. To measure this resonance line one needs a low dephasing rate Γ_{31}, while the line $|mr\rangle \leftrightarrow |rr\rangle$ can be seen in a vast range of dephasing rates.

Up to now there is not much experimental data of the pair correlation function $g^{(2)}(r)$, since it is difficult to achieve spatial resolution. However, a promising method was suggested in [Gün11], so that the resonance lines can be verified in the near future, hopefully. Maybe a possible experiment for the indirect measurement of the resonances could be applied in a similar way as in [Amt10], where an amplification of excitation, the antiblockade effect [Ate07a], was measured. Other methods on how to obtain spatial resolution have been described in [C S06; Tau10; SSR11]. We also note that some simulations for $g^{(2)}$ have already been done, such as in [RH05; HR06; SC10].

The situation which was considered here would require an experimental apparatus to resolve about 100 nm, which is less than the diffraction limit and might be too difficult.

However, for larger values of C_6 the absolute difference of the two resonance lines can be increased. We chose a rather small C_6 value here in order to apply the Hybrid model: As pointed out in section 5.1.2, pair effects like 2-photon-excitation are only included up to a critical length which depends on the density. For a larger C_6 and the same (or even a higher) density, the interesting resonances would not be covered by the pairs in the Hybrid model anymore.

7.4 Counting Statistics

An interesting method to prove the evidence of the Rydberg blockade was introduced by [Lie05]: The blockade limits the number of excitations in the gas and for certain settings it is approximately given by $V/(\frac{4}{3}\pi R_b^3)$, where R_b is the blockade radius. In this case the fluctuation during several realizations should be small. This can be quantified by the so called Q parameter.

The Mandel Q parameter is defined as [Man79]:

$$Q = \frac{\langle N_R^2\rangle - \langle N_R\rangle^2}{\langle N_R\rangle} - 1 \tag{7.8}$$

with $N_R = \sum_{i=1}^{N} |r\rangle^{(i)(i)}\langle r|$. Its value gives the statistics of counting Rydberg excitations: zero, negative and positive for a Poissonian, sub-Poissonian and super-Poissonian distribution, respectively.

The derivation for Q the case of non-interacting, independent atoms can be found in [HR06]:

$$Q_{\text{uncorrelated}} = -\rho_{rr} \tag{7.9}$$

Here ρ_{rr} is the Rydberg excitation probability. So even for uncorrelated atoms the counting statistic is sub-Poissonian. For the interacting case calculations using a rate equation model [Ate06] and many-body Hamiltonians [HR06] were performed and showed a strong sub-Poissonian character.

This has been measured in [Lie05], but the results were withdrawn in [Lie07]. In experiments one not only has to deal with the fluctuation in Rydberg excitations, but also in the total number of atoms. Thus, it is not easy to obtain the real value for Q. In [RYR08], however, the sub-Poissonian behaviour could be measured.

With our models we can easily calculate the Mandel Q parameter: the numerator in equation 7.8 is the variance of N_R. Thus, in the case of the Hybrid model and the rate equation, we have to run our simulation several times and produce a histogram with respect to the Rydberg excitation number. The histogram's mean and variance then give the Q parameter. Note that Q is a $g^{(2)}$-type observable, that means we cannot use the fast evaluation method of section 4.1.3 here. The cluster expansion model has also access to this observable: because two-atom correlations are included exactly, it can give values for $\langle N_R^2\rangle$. However, it cannot produce a histogram. The mean-field model cannot be used to calculate the Q parameter, because like in the pair correlation case, it has no information about two-particle correlations.

The behaviour of Q can be seen in figure 7.9. Here Q was calculated with the rate equation and the cluster expansion. It is very different from the uncorrelated case (dashed line) and shows sub- as well as super-Poissonian parts. At resonance $\Delta = 0$ we see the expected sub-Poissonian statistics of Rydberg counts. Interestingly, for positive detuning Q becomes positive, that means in an experiment one would see a strong fluctuation

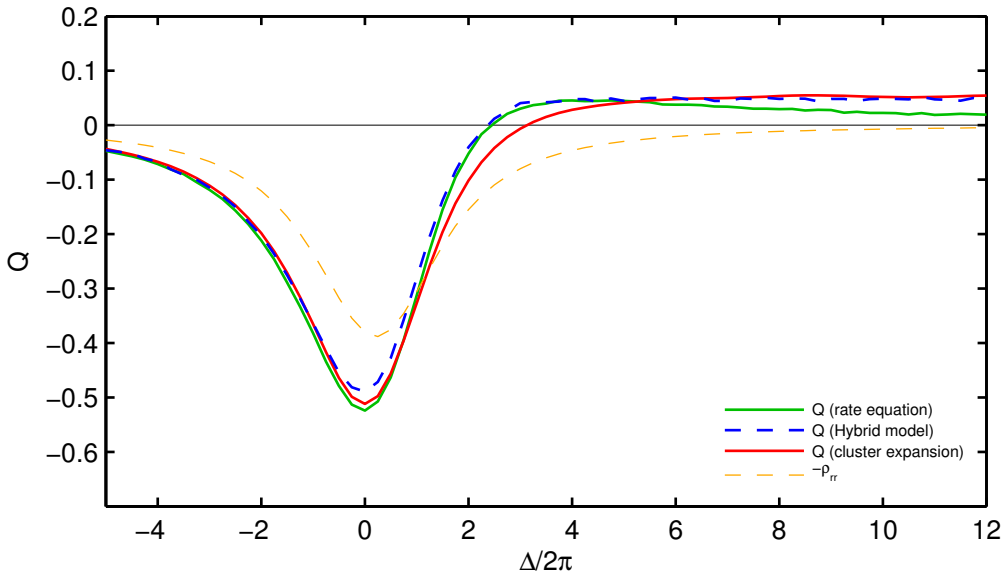

Figure 7.9: Mandel Q parameter in a 3-d trap. Sub- and super-Poissonian statistics can be seen. Q is clearly different from $Q_{\text{uncorrelated}} = -\rho_{rr}$. Parameters: $\Omega_{12} = 3{\cdot}2\pi, \Omega_{23} = 3{\cdot}2\pi, \gamma_{21} = 6{\cdot}2\pi, \gamma_{32} = 1/40{\cdot}2\pi, C_6 = 310000, n_{3\text{D}} = 10^{-3}$.

of Rydberg counts.

We also performed a simulation with a lattice geometry (fig. 7.10) where we used both the rate equation and the Hybrid model, the latter one with the pair structure from figure 5.5. As seen in section 7.1, the cluster expansion is not very well suited for a lattice structure in general, but nevertheless we use it in our discussion here. We used the same parameter as in figure 7.9 but changed to interaction strength such that neighbouring atoms see an interaction of $V_{\text{NN}} = 10 \cdot 2\pi$. The super-Poissonian part is even more pronounced compared to the simulation for the 3-d random sample. Interestingly, the rate equation and the Hybrid model show big differences in the histogram at $\Delta_{23} \approx 5{\cdot}2\pi$, but the Q-parameter is not affected by this. Both of them show a large super-Poissonian part around $\Delta \approx V_{\text{NN}}$, which leads to the assumption that super-Poissonian statistics occur when a double excitation resonance is present. Also the cluster expansion model yields this maximum at V_{NN}, but in addition at $\Delta = V_{\text{NN}}/2$ which corresponds to the $|mm\rangle \leftrightarrow |rr\rangle$ process. Presumably, the effect is not seen in the case of the Hybrid model simulation due to overlapping pairs in the particle treatment. In order to check if the super-Poissonian part at $V_{\text{NN}}/2$ can be obtained with the Hybrid model at all, we change the interaction energy to $V_{\text{NN}} = 100 \cdot 2\pi$ and calculate Q in the range of $-20 \leq \Delta/2\pi \leq 120$. This is equivalent to the case where we divide all parameters by a factor of 10 and keep the interaction strength at $10 \cdot 2\pi$. Then we can in fact observe both resonances with this second set of parameters. This shows that the Hybrid model is in principle capable of producing this feature.

In order to explain the occurrence of the super-Poissonian part we introduce an alternative formula for the Q parameter: It can be expressed in terms of the pair correlation function $g^{(2)}(r)$. A detailed derivation can be found in [Ate09]. If we use the assumption that the Rydberg excitation probability ρ_{rr} is independent of the atoms' positions, we

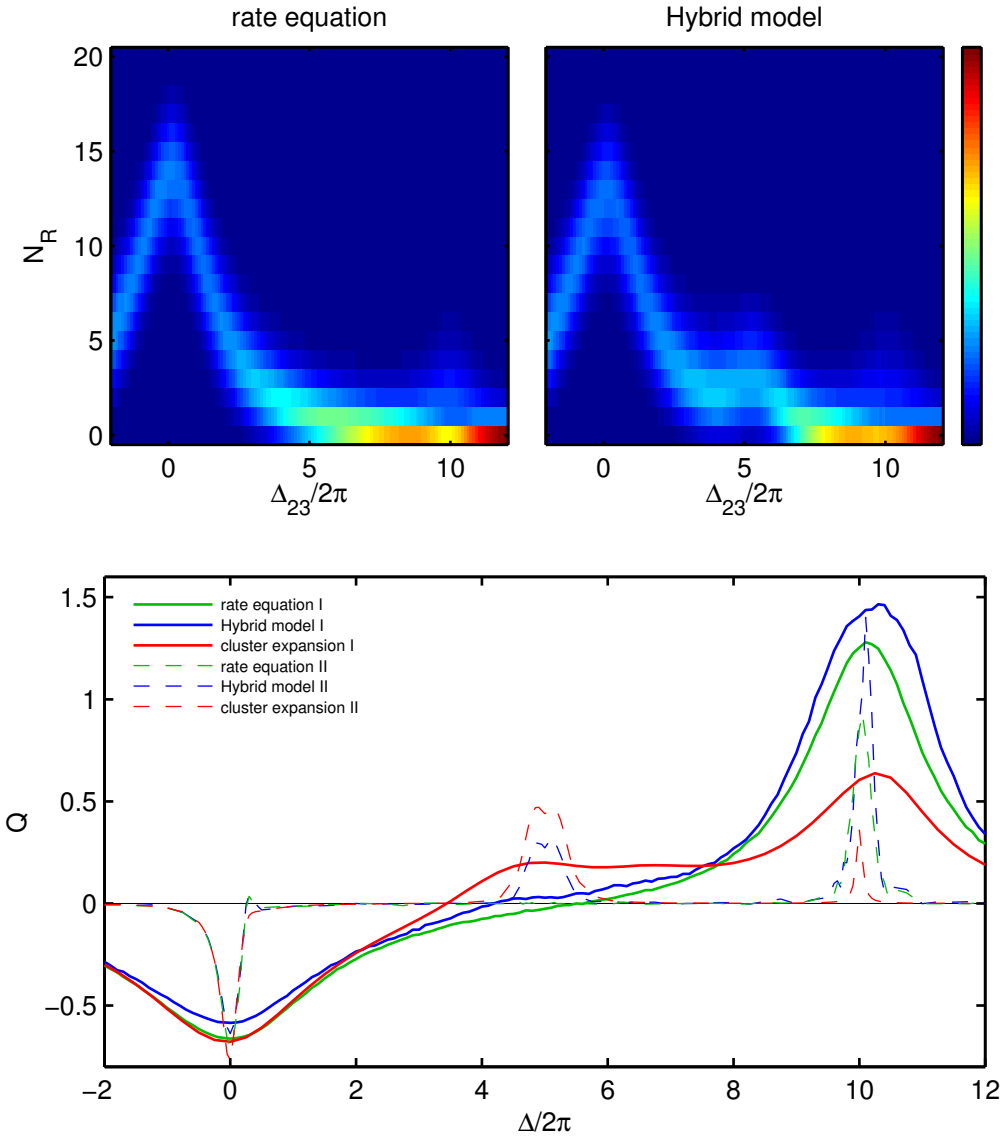

Figure 7.10: Q parameter on a lattice with two different sets of parameters. The statistics are super-Poissonian at $\Delta = V$ and $\Delta = V/2$. Histograms are calculated with parameter set I.

obtain:

$$Q = \frac{N\rho_{rr}}{V^2} \int d^3r d^3r' \left(\frac{N-1}{N} g^{(2)}(|\vec{r} - \vec{r}'|) - 1 \right) \tag{7.10}$$

Indeed, both calculation techniques for Q show the same result in our simulations. A numerical problem might occur if the pair correlation function $g^{(2)}$ is only known up to a certain R and not to the maximal length in the trap. In these cases $g^{(2)}$ has to be extrapolated, which sometimes gives different results in the resulting value for Q. In the case of a 1-d lattice structure the expression 7.10 can be simplified a lot. Here the pair correlation function $g^{(2)}$ is not continuous, but has discrete values at the positions $n \cdot a$,

where a is the lattice constant. We find:

$$Q_{\text{1-d lat.}} = \rho_{rr} \sum_{n=1}^{N} \left(\frac{2(N-n)}{N} g^{(2)}(n \cdot a) - 1 \right) - \rho_{rr} \tag{7.11}$$

Note that both the relations 7.10 and 7.11 give $Q = -\rho_{rr}$ in the case of no correlation, that means $g^{(2)} \equiv 1$, just as claimed in equation 7.9.

With this connection between Q and $g^{(2)}(r)$ we can explain the super-Poissonian parts of the simulations. In fig. 7.10 the maximum is at $\Delta = 10$ which is the potential of two neighbouring atoms. This is also the condition for the resonance in $g^{(2)}$ (see 7.6). This means that the value for $g^{(2)}(a)$ in equation 7.11, and therefore Q, becomes very large.

In the case of a 3-d geometry (fig. 7.9) the same explanation holds: For a positive detuning the integral in 7.10 contains contributions of the large values from $g^{(2)}$. In a random sample we have many distances and thus the main peak of Q is smeared over a large range of detunings. Moreover, the Hybrid model and the cluster expansion contain the 2-γ-resonance and thus the super-Poissonian parts are slightly larger than in the case of the rate equation model.

To sum up: The high correlation between Rydberg atoms can be seen in the Q parameter. For zero detuning the excitation statistics are highly sub-Poissonian as expected. However, the Q parameter also has parts where it becomes larger than zero, which means the excitation count fluctuates stronger than a Poissonian distribution. On a lattice these ranges coincide with the channels for resonant multiple Rydberg excitations.

8 Summary

The strong interaction between Rydberg atoms has led to extensive studies of many-body effects during the last years. For example, schemes from quantum optics like EIT and CPT [Pri10; Sch10] as well as gate protocols from quantum information theory [Luk01] have drawn a lot of attention to both experimental and theoretical works in this field. Effects like the dipole blockade often give an intuitive picture of understanding of the basic properties. In the last few years, the rapid development of experimental techniques and the increase in computational power has led to many possibilities of studying more complicated aspects in many-body Rydberg physics. However, it is still largely unexplored what correlation signatures are inherent in Rydberg gases. It is therefore of interest to develop new numerical methods in order to investigate the properties of such many-body systems. In this thesis we discussed the Rydberg-Rydberg interaction and analysed several models which describe clouds of Rydberg atoms in detail.

The exponential scaling laws with respect to the atom number N of a straightforward many-body simulation demands the use of more sophisticated models. One way is to omit certain states in the Hilbert space, which are not populated at any time, in order to reduce the dimension of the system of differential equations. We call these models many-body Hamiltonian calculations. The focus of this work are different kinds of approaches: Instead of solving the Schrödinger equation with all correlations, it is sometimes possible to start with a few-atom description. This system can then be expanded to a larger number of atoms by truncating the correlations at a given order or by using approximate expressions of the interaction potential.

Several of such simplified models are present in the literature. The earliest experiments could be described with mean-field models [Ton04], which use the presumption of no correlation at all. The expansion of including two-particle correlations was done in [Sch10] (cluster expansion). A different type of model is the rate equation [Ate07b]. By using an approximate description for the interaction, the basic equations are brought into a form which can be solved with Monte Carlo techniques.

We implemented these existing models and accelerated their runtime. In the case of the cluster expansion we exploited, amongst others, the fact that two atoms starting from a certain distance behave uncorrelated. Instead of $\frac{1}{2}N(N-1)$ possible pairs of atoms which had to be included in the simulation, we could thus reduce this number to a linear scaling in N. This procedure decreased the number of variables in the system of differential equations and lowered the runtime considerably. The rate equation model is often not capable of calculating the physical trajectory, but only the steady state of the system. In this case we found that we can use the single-atom steady state values to calculate the jump probabilities for the Monte Carlo method. By this, the rate equation is universally useable over a vast range of parameters. We also used a time independent Monte Carlo algorithm to speed up the simulation and described a method how to obtain faster results for most observables.

In addition, we presented a new model, which is based on the rate equation. The rate equation itself does not include the interaction in an exact manner which already appears in two-body calculations. Effects like a two-photon transition are not covered.

Therefore, we started at a two-atom level to include exact pair correlations in the model. It turned out that we have to mix single- and two-atom descriptions in our simulations to obtain the closest result to the exact solution. Thus, we call this technique the Hybrid model. The Hybrid model can benefit from all the speed improvements we made for the rate equation and can give exact two-particle correlations up to a certain distance.

Furthermore, we discussed the technical properties of these four models. It turned out that the mean-field model does not give reasonable results for few atoms or on a lattice structure in general. Moreover, its structure makes it impossible to compute more advanced observables. The cluster expansion is known to break down at high densities. We analysed if a different truncation of correlations could give consistent high density results for this model. Thereby, we noticed that due to the truncation the cluster expansion models can give non-physical results if there is no damping in the system: A pure state does not remain a pure state and probabilities can get negative or larger than one. In the case of the cluster expansion it turns out that the usual damping like spontaneous emission inhibits this effect, while the cluster expansion with the high density addition (SLA) does not give physical results in general. We discussed the possibility of including time dependence to the rate equation and the Hybrid model but found no working ansatz. In addition, we analysed the problem of "overlapping pairs" in the Hybrid model, which reduces the accuracy of the gained advantage to the rate equation. We also examined the models' capabilities in terms of atom numbers N. To this end we looked at scaling of the runtime as a function of N in detail.

In the last part of the thesis we applied the models to realistic physical setups and computed several observables. First, we looked at the excitation probability in dependence of the laser detuning. It turned out that the main peak of the spectrum decreases while increasing the density, just as the Rydberg blockade predicts. The mean-field model showed a large shift of the main peak structure, which could be understood in the context of the few-particle results. The cluster expansion showed a very small shift of the resonance, which is probably due to the fact that it breaks down at high densities and underestimates the interaction effects. We also used a lattice geometry setting where the two-photon resonance could be seen for both the Hybrid and the cluster expansion model. The next observable we looked at in detail was the susceptibility, which is related to the laser absorption in an EIT system. We could reproduce the strong density dependence from [ASP11] and observe the breakdown of the cluster expansion model. With the high density additions, however, we could observe that the cluster expansion showed the same structure as the other models, and is consistent with analytical low- and high-density estimations. Next, we discussed the pair correlation function $g^{(2)}$ in detail, which can be calculated with all models except the mean-field model. In dependence of the interaction strength, we found that the blockade radius behaves within our estimates. More interesting is the dependence of the laser detuning. We found that special resonances in the $g^{(2)}$ function occur, if the detuning cancels the interaction induced energy shift. The structure of the main resonance corresponds to a single-atom excitation and is seen for all models. The Hybrid model and the cluster expansion, however, showed the resonance line caused by two-photon process in addition. We also saw that a small dephasing does not change the occurrence of the double peak structure. A third resonance line which arises from three simultaneously excited atoms could be seen with the Hybrid model and the rate equation. Another observable we looked at in detail is the Mandel Q parameter. All considered models with the exception of the mean-field model are capable of computing this quantity. As predicted in [Lie05] we observed that for zero

	mean-field model	cluster expansion (LA)[9]	cluster expansion (SLA)[9]	rate equation	Hybrid model	many-body Hamiltonian [Gär11]
densities	very low	low	medium	medium	medium	high
atoms in blockade volume	1	2	$2^{[1]}$	$1^{[1]}$	$2^{[1]}$	N
number atoms	$\approx 10^{4\,[2]}$	$\approx 10^3$	$\approx 10^2$	$\approx 10^4$	$\approx 10^3$	$\lessapprox 10^2$
exact single particle description	✓	✓	✓	✓	✓	✓[8]
exact two-atom description	-	✓	✓	-	✓	✓[8]
highest order of correlations	1	2	2	1,$N^{[3]}$	$2^{[3]}$,$N^{[4]}$	N
single-atom coherences	✓	✓	✓	✓[5]	✓[5]	✓
two-atom coherences	-	✓	✓	-	✓[4],[5]	✓
time dependent parameters and time evolution	✓	✓	✓	-	-	✓
spatially resolved parameters and results	✓[2]	✓	✓	✓	✓	✓
works without damping	✓	-	-	-[6]	-[6]	✓
can compute Q	-	✓	✓	✓	✓	✓
can compute $g^{(2)}(r)$	-	✓	✓	✓	✓	✓
includes $\|mm\rangle \leftrightarrow \|rr\rangle$	-	✓	✓	-	✓[4]	✓
can calculate histogram	-	-	-	✓	✓	✓
works on lattice geometry	-	✓	✓	✓	✓	✓
speed	fast	medium	slow	fast[7]	medium[7]	slow
method	non-linear ODE	non-linear ODE	non-linear ODE	Monte Carlo	Monte Carlo	linear ODE
effort for implementation	low	medium	medium - high	medium	medium - high	high

[1] gives consistent, but not exact results for higher numbers
[2] only for N-atom mean-field, not effective single-atom equations
[3] only approximate and only for populations
[4] up to L_{Cr}
[5] with fast evaluation method from sec. 4.1.3
[6] works with very small decay rates $\gamma \ll \Omega$
[7] except for $g^{(2)}$-type observables combined with low excitation numbers
[8] except for damping effects
[9] might collapse in some situations, see sec. 6.1

detuning the statistics are highly sub-Poissonian. In addition, we found that for positive detuning the Q parameter becomes larger than zero, which indicates super-Poissonian statistics. We could explain this with an analytic connection to the pair correlation function: Whenever a resonance in $g^{(2)}$ occurs, Q gets a big positive contribution. We confirmed this by considering a setting on a lattice geometry, where the resonances of $g^{(2)}$ and thus a positive Q are enhanced.

We remark that the models often made qualitatively different predictions, especially at the different resonance lines in $g^{(2)}$. Even if the experimental accuracy was limited, it should thus be possible to identify the model which is the closest to reality. In general we expect the Hybrid model to be the most precise one, because it includes a higher order of correlation compared to the rate equation and mean-field model and gives reasonable high density results, unlike the cluster expansion.

In order to give a brief overview on the capabilities of the considered models we listed some of their properties in the adjoining table. In addition, we included a column about the many-body Hamiltonian calculations for comparison. Note that we designed the table for the simplified models and thus the limitations of the Hamiltonian calculations (see sec. 2.3.4) are not listed.

With the analysis and comparison of the models in this work it should be easier to decide which models are suited to describe a given experimental setup best.

9 Outlook

In this thesis we considered the interaction between Rydberg atoms in an s-state. Therefore, the interaction is independent of the atoms' orientation. However, if atoms are excited into states with higher angular quantum number like p or d-states, the interaction will depend on the alignment of the dipols. In principle, one could add this angular dependency to the discussed models. This would be important if such atoms are located on a 1-dimensional string and their orientation is controlled with external electric fields. It is also of interest in which cases an effective, orientation independent C_6 coefficient can be used.

Closely related is the effect of super- and subradiant Rydberg states. The discussion from section 3.3 could be expanded to different states and potentially give insight on how to utilize super- or subradiance in Rydberg systems in a controlled way. Moreover, we have seen that the first order calculation might not be enough to describe the collective decay. A numerical study could be performed here.

Also a fundamental change could be applied to the models: The discussed methods work with a classical radiation field. As recent simulations suggested [POF11], a quantized field treatment might be necessary for a full understanding of the EIT features in Rydberg systems in the case of weak probe beams Ω_{12}. It is unclear how this could be included to the existing models, most likely new techniques have to be developed.

The models can also be expanded in a different way: The interaction between Rydberg atoms arises from the dipole coupling to other Rydberg states. In the case of Förster resonances or if the interaction shows a dipole character, it might be required to include these additional states in the simulation, since the strong mixing of the states allows several eigenstates to be populated.

In this thesis we often mentioned exact many-body Hamiltonian calculations. While this method and our discussed models are designed for contrary density regimes, it would be of interest to see how well the extrapolations would agree. The Hamiltonian calculation works without damping, which only allows a steady state comparison with the rate equation, Hybrid or mean-field model with very small decay. As we have seen, the cluster expansion model breaks down at a purely coherent evolution.

Out of our analysis of the pair correlation function several open questions remain. For example, we have seen that $g^{(2)}$ showed some oscillations at zero detuning. These effects are strongly dependent on the parameters: the density, Rabi frequencies, C_6 and the decay rates. It would be interesting to analyse their dependence on the curves' behaviour in view of the forming of a crystalline structure.

It remains an open question if the resonance lines in the pair correlation function and the super- and sub-Poissonian statistics can be seen in an experiment. With the rapidly increasing possibilities this can hopefully be answered in the near future.

Eventually, we note that the models discussed and developed here are not restricted to Rydberg systems. The main requirement is the pairwise interaction between certain states, but the total number of states as well as the nature of the coupling is not relevant. Since the models arise from a master equation it should be possible to include various other effects.

Bibliography

[Aga74] G. S. Agarwal. “Quantum statistical theories of spontaneous emission and their relation to other approaches”. In: *Quantum Optics*. Vol. 70. Springer Tracts in Modern Physics. Springer Berlin/Heidelberg (1974), pp. 1–128.

[Amt08] T. Amthor. “Interaction-Induced Dynamics in Ultracold Rydberg Gases – Mechanical Effects and Coherent Processes”. PhD thesis. Freiburg (2008).

[Amt10] Thomas Amthor et al. “Evidence of Antiblockade in an Ultracold Rydberg Gas”. In: *Phys. Rev. Lett.* **104**, 013001 (2010).

[ASP11] C. Ates, S. Sevinçli, and T. Pohl. “Electromagnetically induced transparency in strongly interacting Rydberg gases”. In: *Phys. Rev. A* **83**, 041802 (2011).

[Ate06] C. Ates et al. “Strong interaction effects on the atom counting statistics of ultracold Rydberg gases”. In: *Journal of Physics B: Atomic, Molecular and Optical Physics* **39**, L233 (2006).

[Ate07a] C. Ates et al. “Antiblockade in Rydberg Excitation of an Ultracold Lattice Gas”. In: *Phys. Rev. Lett.* **98**, 023002 (2007).

[Ate07b] C. Ates et al. “Many-body theory of excitation dynamics in an ultracold Rydberg gas”. In: *Phys. Rev. A* **76**, 013413 (2007).

[Ate09] C. Ates. “Anregungsdynamik ultrakalter Rydberggase”. PhD thesis. Dresden (2009).

[AVG98] W. R. Anderson, J. R. Veale, and T. F. Gallagher. “Resonant Dipole-Dipole Energy Transfer in a Nearly Frozen Rydberg Gas”. In: *Phys. Rev. Lett.* **80**, 249–252 (1998).

[Bon98] M. Bonitz. “Quantum kinetic theory”. Teubner-Texte zur Physik. Teubner (1998).

[Car04] Thomas J. Carroll et al. “Angular Dependence of the Dipole-Dipole Interaction in a Nearly One-Dimensional Sample of Rydberg Atoms”. In: *Phys. Rev. Lett.* **93**, 153001 (2004).

[Cho08] Amodsen Chotia et al. “Kinetic Monte Carlo modeling of dipole blockade in Rydberg excitation experiment”. In: *New Journal of Physics* **10**, 045031 (2008).

[CP10] Daniel Comparat and Pierre Pillet. “Dipole blockade in a cold Rydberg atomic sample [Invited]”. In: *J. Opt. Soc. Am. B* **27**, A208–A232 (2010).

[C S06] C. S. E. van Ditzhuijzen et al. “Simultaneous position and state measurement of Rydberg atoms”. In: *Eur. Phys. J. D* **40**, 13–17 (2006).

[DBW08] J. O. Day, E. Brekke, and T. G. Walker. “Dynamics of low-density ultracold Rydberg gases”. In: *Phys. Rev. A* **77**, 052712 (2008).

[Dem05] Wolfgang Demtröder. “Experimentalphysik 3: Atome, Moleküle und Festkörper”. Springer-Lehrbuch. Springer (2005).

[FIM05] Michael Fleischhauer, Atac Imamoglu, and Jonathan P. Marangos. “Electromagnetically induced transparency: Optics in coherent media”. In: *Rev. Mod. Phys.* **77**, 633–673 (2005).

[FS05] Z. Ficek and S. Swain. “Quantum interference and coherence: theory and experiments”. Springer series in optical sciences. Springer (2005).

[Gaë09] Alpha Gaëtan et al. “Observation of collective excitation of two individual atoms in the Rydberg blockade regime”. In: *Nat Phys* **5**, 115–118 (2009).

[Gal94] Thomas F. Gallagher. “Rydberg atoms”. 1. publ. Cambridge: Cambridge Univ. Press (1994).

[Gär11] Martin Gärttner. private communication (2011).

[Gün11] G. Günter et al. “Interaction enhanced imaging of individual atoms embedded in dense atomic gases”. In: *ArXiv e-prints* (2011). arXiv:1106.5443 [physics.atom-ph].

[Hei08] Rolf Heidemann et al. “Rydberg Excitation of Bose-Einstein Condensates”. In: *Phys. Rev. Lett.* **100**, 033601 (2008).

[HR06] J. V. Hernández and F. Robicheaux. “Coherence conditions for groups of Rydberg atoms”. In: *Journal of Physics B: Atomic, Molecular and Optical Physics* **39**, 4883 (2006).

[Ise10] L. Isenhower et al. “Demonstration of a Neutral Atom Controlled-NOT Quantum Gate”. In: *Phys. Rev. Lett.* **104**, 010503 (2010).

[Jak00] D. Jaksch et al. “Fast Quantum Gates for Neutral Atoms”. In: *Phys. Rev. Lett.* **85**, 2208–2211 (2000).

[Jan03] A. P. J. Jansen. “An Introduction To Monte Carlo Simulations Of Surface Reactions”. In: *ArXiv Condensed Matter e-prints* (2003). eprint: arXiv:cond-mat/0303028.

[Kif10] Martin Kiffner et al. “Vacuum-induced processes in multi-level atoms”. In: *Progress in Optics*. Vol. 55. Burlington: Elsevier Science (2010), pp. 85–197.

[Li03] Wenhui Li et al. “Millimeter-wave spectroscopy of cold Rb Rydberg atoms in a magneto-optical trap: Quantum defects of the ns, np, and nd series”. In: *Phys. Rev. A* **67**, 052502 (2003).

[Lie05] T. Cubel Liebisch et al. "Atom Counting Statistics in Ensembles of Interacting Rydberg Atoms". In: *Phys. Rev. Lett.* **95**, 253002 (2005).

[Lie07] T. Cubel Liebisch et al. "Erratum: Atom Counting Statistics in Ensembles of Interacting Rydberg Atoms [Phys. Rev. Lett. 95, 253002 (2005)]". In: *Phys. Rev. Lett.* **98**, 109903 (2007).

[LTG05] Wenhui Li, Paul J. Tanner, and T. F. Gallagher. "Dipole-Dipole Excitation and Ionization in an Ultracold Gas of Rydberg Atoms". In: *Phys. Rev. Lett.* **94**, 173001 (2005).

[Luk01] M. D. Lukin et al. "Dipole Blockade and Quantum Information Processing in Mesoscopic Atomic Ensembles". In: *Phys. Rev. Lett.* **87**, 037901 (2001).

[Man79] L. Mandel. "Sub-Poissonian photon statistics in resonance fluorescence". In: *Opt. Lett.* **4**, 205–207 (1979).

[MCD93] Klaus Mølmer, Yvan Castin, and Jean Dalibard. "Monte Carlo wave-function method in quantum optics". In: *J. Opt. Soc. Am. B* **10**, 524–538 (1993).

[OGL09] B. Olmos, R. González-Férez, and I. Lesanovsky. "Collective Rydberg excitations of an atomic gas confined in a ring lattice". In: *Phys. Rev. A* **79**, 043419 (2009).

[PAM11] J. D. Pritchard, C. S. Adams, and K. Mølmer. "Correlated photon emission from multi–atom Rydberg dark states". In: *ArXiv e-prints* (2011). arXiv:1108.5165 [quant-ph].

[PDL10] T. Pohl, E. Demler, and M. D. Lukin. "Dynamical Crystallization in the Dipole Blockade of Ultracold Atoms". In: *Phys. Rev. Lett.* **104**, 043002 (2010).

[PM09] Line Hjortshøj Pedersen and Klaus Mølmer. "Few qubit atom-light interfaces with collective encoding". In: *Phys. Rev. A* **79**, 012320 (2009).

[POF11] David Petrosyan, Johannes Otterbach, and Michael Fleischhauer. "Electromagnetically Induced Transparency with Rydberg Atoms". In: *Phys. Rev. Lett.* **107**, 213601 (2011).

[Pri09] J. D. Pritchard et al. "Cooperative optical non-linearity due to dipolar interactions in an ultra-cold Rydberg ensemble". In: *ArXiv e-prints* (2009). arXiv:0911.3523 [quant-ph].

[Pri10] J. D. Pritchard et al. "Cooperative Atom-Light Interaction in a Blockaded Rydberg Ensemble". In: *Phys. Rev. Lett.* **105**, 193603 (2010).

[Res11] Jose Reslen. "Many-body effects in a model of electromagnetically induced transparency". In: *Journal of Physics B: Atomic, Molecular and Optical Physics* **44**, 195505 (2011).

[RH05] F. Robicheaux and J. V. Hernández. "Many-body wave function in a dipole blockade configuration". In: *Phys. Rev. A* **72**, 063403 (2005).

[RYR08] A. Reinhard, K. C. Younge, and G. Raithel. “Effect of Förster resonances on the excitation statistics of many-body Rydberg systems”. In: *Phys. Rev. A* **78**, 060702 (2008).

[SC09] J. Stanojevic and R. Côté. “Many-body Rabi oscillations of Rydberg excitation in small mesoscopic samples”. In: *Phys. Rev. A* **80**, 033418 (2009).

[SC10] J. Stanojevic and R. Côté. “Many-body dynamics of Rydberg excitation using the Ω expansion”. In: *Phys. Rev. A* **81**, 053406 (2010).

[Sch04] F. Schwabl. “Quantenmechanik (QM I): Eine Einführung”. 7th ed. Springer-Lehrbuch. Springer (2004).

[Sch10] H. Schempp et al. “Coherent Population Trapping with Controlled Interparticle Interactions”. In: *Phys. Rev. Lett.* **104**, 173602 (2010).

[Sev11a] S. Sevinçli et al. “Nonlocal Nonlinear Optics in Cold Rydberg Gases”. In: *Phys. Rev. Lett.* **107**, 153001 (2011).

[Sev11b] S. Sevinçli et al. “Quantum interference in interacting three-level Rydberg gases: coherent population trapping and electromagnetically induced transparency”. In: *Journal of Physics B: Atomic, Molecular and Optical Physics* **44**, 184018 (2011).

[Sin04] Kilian Singer et al. “Suppression of Excitation and Spectral Broadening Induced by Interactions in a Cold Gas of Rydberg Atoms”. In: *Phys. Rev. Lett.* **93**, 163001 (2004).

[Sin05] Kilian Singer et al. “Long-range interactions between alkali Rydberg atom pairs correlated to the ns–ns, np–np and nd–nd asymptotes”. In: *Journal of Physics B: Atomic, Molecular and Optical Physics* **38**, S295 (2005).

[SK11] Hans-Rudolf Schwarz and Norbert Köckler. “Numerische Mathematik”. 8th ed. Vieweg + Teubner (2011).

[SSR11] A. Schwarzkopf, R. E. Sapiro, and G. Raithel. “Imaging Spatial Correlations of Rydberg Excitations in Cold Atom Clouds”. In: *Phys. Rev. Lett.* **107**, 103001 (2011).

[Ste07] S. V. Stepkin et al. “Radio recombination lines from the largest bound atoms in space”. In: *Monthly Notices of the Royal Astronomical Society* **374**, 852–856 (2007).

[SW02] M. Saffman and T. G. Walker. “Creating single-atom and single-photon sources from entangled atomic ensembles”. In: *Phys. Rev. A* **66**, 065403 (2002).

[SWM10] M. Saffman, T. G. Walker, and K. Mølmer. “Quantum information with Rydberg atoms”. In: *Rev. Mod. Phys.* **82**, 2313–2363 (2010).

[SZ97] M. O. Scully and M. S. Zubairy. “Quantum optics”. Cambridge University Press (1997).

[Tau10] Atreju Tauschinsky et al. “Spatially resolved excitation of Rydberg atoms and surface effects on an atom chip”. In: *Phys. Rev. A* **81**, 063411 (2010).

[Ton04] D. Tong et al. “Local Blockade of Rydberg Excitation in an Ultracold Gas”. In: *Phys. Rev. Lett.* **93**, 063001 (2004).

[Urb09] E. Urban et al. “Observation of Rydberg blockade between two atoms”. In: *Nat Phys* **5**, 110–114 (2009).

[Vit11] M. Viteau et al. “Rydberg atoms in one-dimensional optical lattices”. In: *ArXiv e-prints* (2011). arXiv:1103.4232 [cond-mat.quant-gas].

[Vog06a] Thibault Vogt et al. “Dipole Blockade at Förster Resonances in High Resolution Laser Excitation of Rydberg States of Cesium Atoms”. In: *Phys. Rev. Lett.* **97**, 083003 (2006).

[Vog06b] Thibault Vogt. “Blocage dipolaire de l’excitation d’atomes froids vers des états de Rydberg: Contrôle par champ électrique et par résonance de Förster”. PhD thesis. Université Paris Sud - Paris XI (2006).

[Wan07] T. Wang et al. “Superradiance in ultracold Rydberg gases”. In: *Phys. Rev. A* **75**, 033802 (2007).

[Wei08] Hendrik Weimer et al. “Quantum Critical Behavior in Strongly Interacting Rydberg Gases”. In: *Phys. Rev. Lett.* **101**, 250601 (2008).

[Wei10] Hendrik Weimer et al. “A Rydberg quantum simulator”. In: *Nat Phys* **6**, 382–388 (2010).

[Whi11] Shannon Whitlock. private communication (2011).

[Wüs10] S. Wüster et al. “Correlations of Rydberg excitations in an ultracold gas after an echo sequence”. In: *Phys. Rev. A* **81**, 023406 (2010).

[You09] K. C. Younge et al. “Mesoscopic Rydberg ensembles: Beyond the pairwise-interaction approximation”. In: *Phys. Rev. A* **79**, 043420 (2009).

Acknowledgements

Mein ganz besonderer Dank gilt meinem Betreuer PD Dr. Jörg Evers, der mir erst ein Projektpraktium und dann die Diplomarbeit über die Rydbergmodelle in seiner Gruppe ermöglicht hat. Du hast mir von Anfang an großes Vertrauen entgegengebracht, mich motiviert und inspiriert. Auch für deine immer offene Tür bei Fragen möchte ich mich bedanken. Ebenfalls vielen Dank an Prof. Keitel, der mir die Teilnahme an der DPG-Tagung in Dresden ermöglichte.

Zu ganz großem Dank verpflichtet bin ich auch Martin Gärttner, meinem Mitstreiter in Sachen Rydbergmodellen. Die vielen Diskussionen und der unmittelbare Austausch von unseren Ergebnissen war mir eine unschätzbare Hilfe.

An dieser Stelle möchte ich auch all meinen Bürogenossen für die tolle Atmosphäre danken und ebenso meinen Freunden und Kollegen aus der Abteilung für die schöne und angenehme Zeit.

Nicht zuletzt gilt mein Dank meiner Famile und meinen Freunden für die vielfältige Unterstützung. Ihr seid die Besten! Ebenfalls vielen Dank an diejenigen, die mir beim Korrekturlesen dieser Arbeit geholfen haben.

Zum Schluss möchte ich noch alle grüßen, die mich kennen ;-)

Erklärung:

Ich versichere, dass ich diese Arbeit selbstständig verfasst habe und keine anderen als die angegebenen Quellen und Hilfsmittel benutzt habe.

Heidelberg, den 20.12.2011 .....